ADVANCED ENERGY MATERIALS
www.advenergymat.de

Progress in Aqueous Rechargeable Sodium-Ion Batteries

Duan Bin, Fei Wang, Andebet Gedamu Tamirat, Liumin Suo, Yonggang Wang, Chunsheng Wang, and Yongyao Xia**

Sodium (Na) is one of the more abundant elements on earth and exhibits similar chemical properties as lithium (Li), indicating that Na could be applied to a similar battery system. Like aqueous Li-ion batteries, aqueous sodium-ion batteries (ASIBs) are also demonstrated to be one of the most promising stationary power sources for sustainable energies such as wind and solar power. Compared to traditional nonaqueous batteries, ASIBs may solve the safety problems associated with the highly toxic and flammable organic electrolyte in the traditional lithium-ion and sodium-ion batteries. During the past decades, many efforts are made to improve the performance of the ASIBs. The present review focuses on the latest advances in the exploration and development of ASIB systems and related components, including cathodes, anodes, and electrolytes. Previously reported studies are briefly summarized, together with the presentation of new findings based on the electrochemical performance, cycling stability, and morphology approaches. In addition, the main opportunities, achievements, and challenges in this field are briefly commented and discussed.

1. Introduction

Our planet faces energy sustainability challenges that call for intensive researches in various disciplines, including the field of electrochemical energy storage derived from solar, wind, and tidal power.[1] Thus, substantial progress in battery technology is the center of attention to store electricity in large scale among the various energy storage technologies, due to its flexibility, high energy conversion efficiency, and simple maintenance. Among various electrochemical grid-scale energy storage systems (ESSs) that shown in **Figure 1**, the secondary battery technique is one of the promising choices for hybrid electric vehicles and plug-in hybrid electric vehicles that can store electricity on a large scale and reduce dependence on fossil fuels.[2–4] To this end, long cycle life, low cost, eco-friendly, and high safety are the most important parameters for ESSs. Currently, Li-ion batteries (LIBs), flow batteries like Ni–MH, Ni–Cd and Pb–acid, $Na/NiCl_2$, Na–S, Li–O_2, and Li–S batteries have been considered as potential energy storage devices for ESSs.[5–7] The flow batteries like Ni–MH, Ni–Cd, and Pb–acid were feasible in past, whereas the environment pollution and safe risk caused by these batteries have deviated away from the parameters of ESSs. Although the Li–O_2 and Li–S batteries appear to offer the great hope for ESSs by virtue of extremely high energy density, the extensive material challenges and barriers involving electrodes, electrolytes, interfaces, and additive materials could have a profound effect on stabilizing electrode–electrolyte interactions.[8]

The practical application of Li-ion batteries has attracted enormous attention and realized in portable devices due to their high energy density and long cycle, and the Li-ion aqueous systems can be a possible substitute for conventional aqueous rechargeable systems such as Ni–MH, Ni–Cd, and Pb–acid since the first aqueous Li-ion battery (ALIB) developed by Dahn and coworkers in 1994.[9–11] However, there are some intrinsic characteristics including the growing price of Li resources and safety to make the current LIBs less attractive for large-scale stationary ESSs.

Compared with Li, sodium (Na) is the sixth most abundant element in the earth's crust, making it be investigated as a guest ion to develop less expensive and easy accessibility of Na rechargeable battery systems. The early research has focused on high-temperature Na rechargeable battery systems such as $Na/NiCl_2$ and Na–S batteries, but the safety issue of molten Na and sulfur at 300–350 °C in Na–S batteries is also a remarkable problem for large-scale applications.[6] Aqueous sodium-ion batteries (ASIBs) offer multiple advantages such as wide abundance in the earth's crust, a

Dr. D. Bin, Dr. A. G. Tamirat, Prof. Y. Wang, Prof. Y. Xia
Department of Chemistry and Shanghai Key Laboratory of Molecular Catalysis and Innovative Materials
Institute of New Energy
iChEM (Collaborative Innovation Center of Chemistry for Energy Materials)
Fudan University
Shanghai 200433, China
E-mail: yyxia@fudan.edu.cn

Dr. F. Wang, C. Wang
Department of Chemical and Biomolecular Engineering
University of Maryland
College Park, MD 20742, USA
E-mail: cswang@umd.edu

Dr. L. Suo
Department of Nuclear Science and Engineering
Massachusetts Institute of Technology
Cambridge, MA 02138, USA

DOI: 10.1002/aenm.201703008

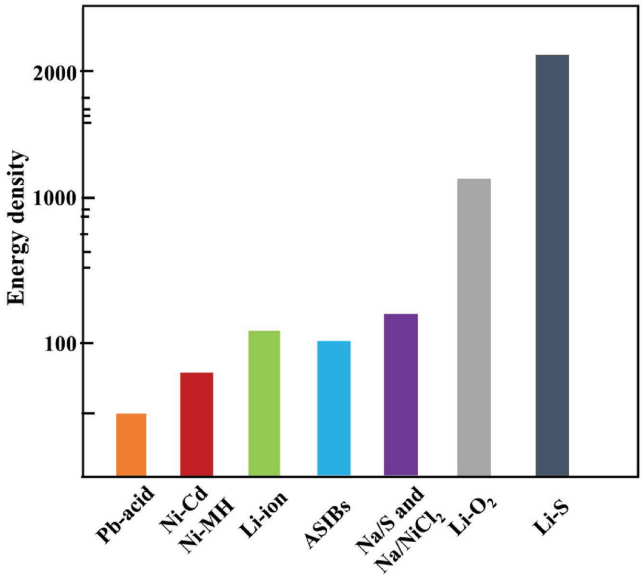

Figure 1. Graph of energy density of various energy storage systems.

seemingly unlimited distribution, and distinctly lower cost of Na; hence they are recognized as serious alternative to Na-ion batteries.[12–14] Moreover, the traditional organic-electrolyte-based Na-ion battery, which uses highly toxic and flammable solvent, can cause safety hazards when used improperly. In contrast, in terms of nonflammability, fast ion transportation, and lower manufacturing cost, ASIB is deemed to be most suitable for large-scale stationary ESS applications.

Despite the identical mechanism of ASIBs to that of conventional organic battery, the electrochemical reaction of Na^+ extraction/insertion in aqueous electrolyte is more complicated, thereby leading to a great influence on selectivity of electrode materials. First, the redox potentials of electrode materials in aqueous electrolyte should be within or near the electrolysis potentials of water, beyond which the electrolysis of H_2O occurs with H_2 or O_2 evolution. Second, the side reactions between electrode materials and H_2O or residual O_2 will tremendously affect their cyclic stability. In addition, proton coinsertion into the host electrode materials and electrode dissolution have substantial roles in the performance and cycling life of aqueous electrolyte systems. Although the previous reports have elaborated the aqueous rechargeable alkali-metal-ion (Li^+, Na^+) batteries that are promising alternatives for large-scale applications by 2014, some other potential materials and perspective for electrolyte come out currently.[3] In this review, we introduce detailed summaries of electrode materials (both cathodes and anodes) including oxides, polyanionic compounds, and their derivatives, Prussian blue analogs, and organic compounds, which have been most extensively reported for use in ASIBs. We also make a systematic comparison between the diluted and concentrated electrolytes in ASIBs, it is concluded that the shortcomings of some electrode materials could be virtually eliminated by employing concentrated electrolytes, in which the water activity is strongly suppressed.

Duan Bin received his M.S. degree in the College of Chemistry, Chemical Engineering and Materials Science of Soochow University in 2016. Now he is working toward a Ph.D. degree in Department of Chemistry, Fudan University. His current research is focused on energy-storage materials and aqueous rechargeable batteries.

Chunsheng Wang is a Professor in the Chemical and Biomolecular Engineering at the University of Maryland. He is a UMD Director of the ARL-UMD Center for Research in Extreme Battery. He received his Ph.D. in Materials Science and Engineering from Zhejiang University, China, in 1995. His research focuses on reachable batteries and fuel cells. His work on lithium batteries have been featured in NASA Tech Brief, EFRC/DoE newsletter, C&EN, etc.

Yongyao Xia is a Professor in the Department of Chemistry and Institute of New Energy of Fudan University. He received a Bachelor of Science degree from the Chemistry Department of Zhejiang Normal University in 1987 and a Master of Science degree in Electrochemistry from the Chemistry Department of Jilin University in 1990. He received a Ph.D. degree in Energy-Related-Material Science in Saga University, Japan, in 1997. His research interests involve advanced materials and technologies for energy storage and conversion devices, e.g., lithium-ion batteries, sodium-ion batteries, electrochemical supercapacitors, lithium–air, and lithium–sulfur batteries.

2. Cathode Materials

Obviously, the ASIBs have been displaying a great potential to be utilized as a green, safe, and low-cost power sources for grid-scale energy storage applications. However, the fundamental work condition of ASIBs depends on the intercalation

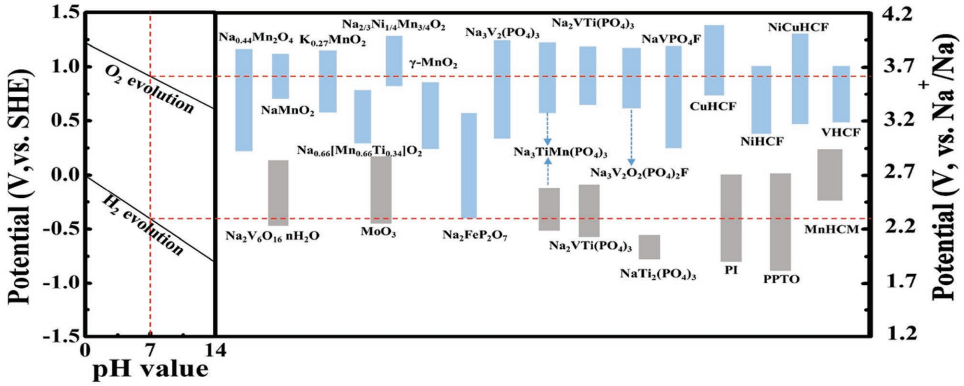

Figure 2. Electrochemical stability window of aqueous elelctrolyte with different pH values and the redox potential for the electrode materials in ASIBs.

of Na ions in water-based environment. **Figure 2** shows the relationship between the hydrogen and oxygen evolution (left) and the applied extraction/insertion potential of Na ion (right). The detailed electrochemical performance of these materials for application in ASIBs will be discussed in the following sections.

2.1. Mn-Based Oxides

Similar to aqueous rechargeable lithium-ion batteries, pioneering researchers have tried to use transition metal oxides as cathode material, including V_2O_5, MnO_2, and RuO_2.[15–17] However, these types of metal oxide electrodes typically have capacitance behavior, which undergo the Faraday adsorption and desorption processes on their surfaces, instead of Na-ion extraction/insertion reaction. Previously, the variation of birnessite-type δ-MnO_2 structure, a 2D layer-structure material, was reported by Athouel et al. It has presented a charge/discharge behavior in aqueous Na_2SO_4 electrolyte which has delivered a stable capacitance of 145 F g^{-1} over 50 cycles (**Figure 3**a).[18] Recently, Whitacre et al. have found that cubic spinel λ-MnO_2 has excellent energy storage property in aqueous Na_2SO_4 solution.[19] Figure 3b depicts that λ-MnO_2 could achieve the discharge capacity of ≈80 mA h g^{-1}, over the previously described orthorhombic $Na_4Mn_9O_{18}$ material. When they used λ-MnO_2 cathode and activated carbon (AC) anode electrode materials as a thin coin cell, 70% of the theoretical capacity was achieved without capacity loss up to 5000 cycles (Figure 3c). These results show that cubic spinel λ-MnO_2 could effectively be functional in a neutral pH Na_2SO_4 solution. In addition, the reason

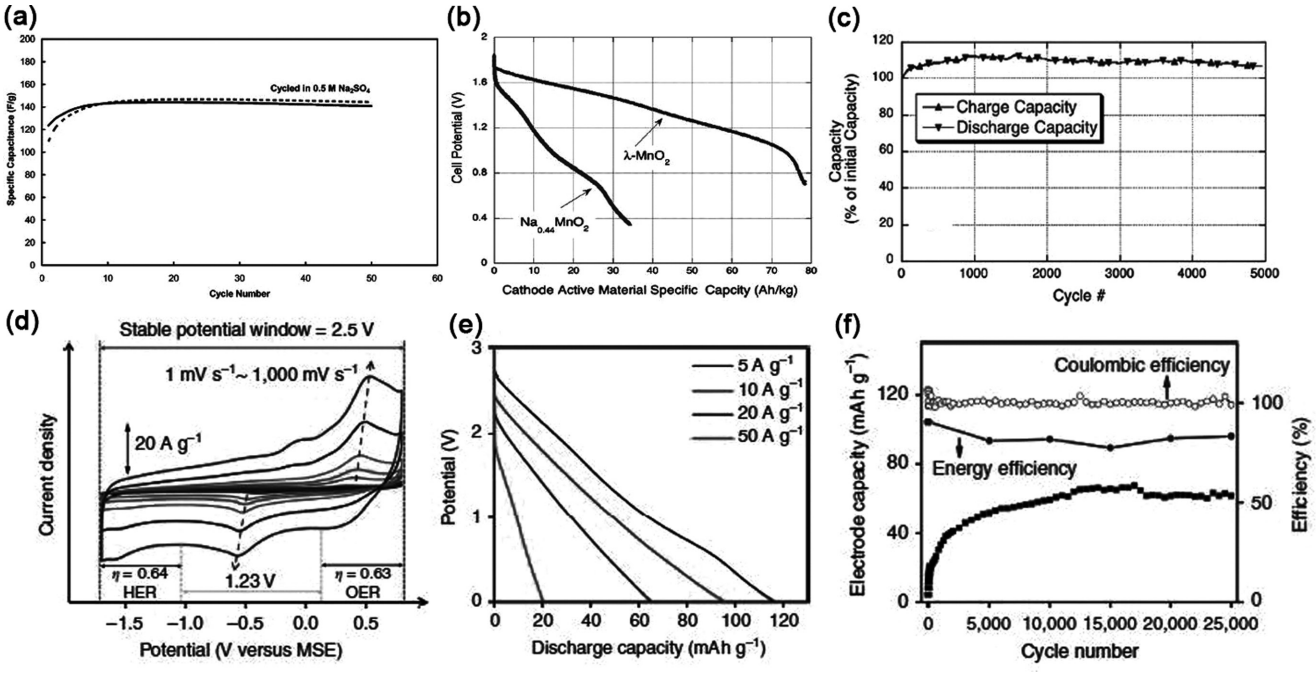

Figure 3. a) Charge/discharge capacity evolution of Mg-doped Na-birnessite electrode during 50 cycles at 2 mV s^{-1} in 0.5 M Na_2SO_4 electrolyte. Reproduced with permission.[18] Copyright 2008, ACS. b) Discharge curves of $Na_4Mn_9O_{18}$ and λ-MnO_2 in 1 M Na_2SO_4 solution. c) High rate cycle life testing on a thin λ-MnO_2/AC full cells up to 5000 cycles. Reproduced with permission.[19] Copyright 2012, Elsevier. d) CVs show a stable potential window of Mn_5O_8 and large overpotential toward HER and OER. e) Discharge capacity of Mn_5O_8 electrode at different current densities. f) Mn_5O_8 electrode capacity and Coloumbic efficiencies as functions of cycle number at 20 A g^{-1}. Reproduced with permission.[20] Copyright 2016, Macmillan Publishers Ltd.; Nature Communications.

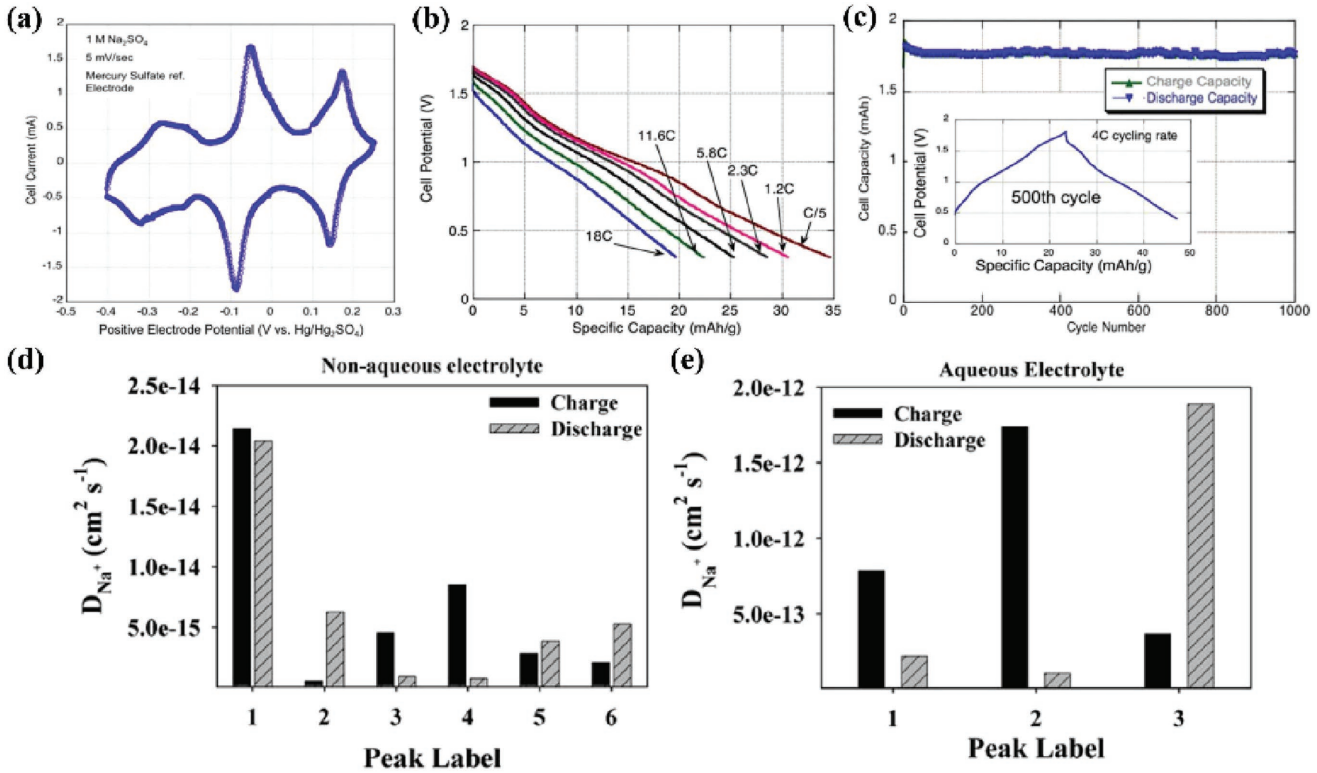

Figure 4. a) CV curve (5 mV s^{-1}) with $Na_{0.44}MnO_2$ as the working electrode material in 1 M Na_2SO_4 solution, versus $Hg/HgSO_4$ reference electrode. b) $Na_{0.44}MnO_2$/AC cell potential as a function of specific capacity under a range of discharge currents. c) Cell charge and discharge capacity as a function of cycle number for 4 C galvanostatic cycling with a potential window of 0.4–1.8 V. Reproduced with permission.[21] Copyright 2010, Elsevier. Diffusion coefficient values of Na^+ ion at the peak positions in d) nonaqueous and e) aqueous electrolytes. Reproduced with permission.[22] Copyright 2013, Elsevier.

of excellent performance for representative materials was summarized in this paper, which could account for high-surface-area carbons and the thin electrode devices. Most recently, a high-rate high-voltage aqueous Na-ion full cell system based on a surface hydroxylated Mn_5O_8 electrode was first reported by Shan et al.[20] As shown in Figure 3d, the Mn_5O_8 nanoparticles showed a wide potential window between −1.7 (0.64 V overpotential for hydrogen evolution reaction (HER)) and 0.8 V vs Hg/Hg_2SO_4 (0.64 V overpotential for oxygen evolution reaction (OER)) in 0.1 M Na_2SO_4 electrolyte, demonstrating sluggish OER and HER reactions, thereby leading to a stable 2.5 V potential window in an aqueous Na-ion half-cell. Figure 3e displays discharge capacity of Mn_5O_8 electrode at different current densities ranging from 5 to 50 A g^{-1}. A capacity of ≈116 mA h g^{-1} was obtained at 5 A g^{-1}, and up to 20 mA h g^{-1} was maintained at 50 A g^{-1}. Figure 3f shows better cycling stability of Mn_5O_8 full cells measured at 20 A g^{-1}. The Mn_5O_8 cell exhibited excellent Coulombic (≈100%) and energy efficiency (≈85%), and a plausible electrode capacity of 61 mA h g^{-1} after 25 000 cycles. Noticeably, this system exhibited a two-electron charge transfer via Mn^{2+}/Mn^{4+} redox couple and provided a facile pathway for Na-ion transport through the intra/interlayer defects of Mn_5O_8.

In the following years, Whitacre et al. have demonstrated a tunnel structural $Na_{0.44}MnO_2$ (NMO) material, which presented three redox potentials (–0.3 to 3 V vs Hg/Hg_2SO_4) in 0.1 M Na_2SO_4 solution as revealed in **Figure 4**a, clearly indicating the formation of multiphase behavior on the Na-ion extraction/insertion process.[21] Although the $Na_{0.44}MnO_2$ material could only deliver a specific capacity of ≈35 mA h g^{-1} at C/5 rate, it can still maintain up to 20 mA h g^{-1} at 18 C rate (Figure 4b). In addition, the full cell $Na_{0.44}MnO_2$ /activated carbon configuration, ranged from 0.4 to 1.8 V, displayed outstanding stability after 1000 charge/discharge cycles at 4 C (Figure 4c). The excellent cycling performance confirms that the material is promising for cathode electrode material in ASIBs. The Na-ion intercalation and de-intercalation behavior of $Na_{0.44}MnO_2$ have also been investigated by Kim et al.[22] They have shown that $Na_{0.44}MnO_2$ demonstrates better rate capability in the aqueous system than the nonaqueous one. As manifested in Figure 4d,e, the apparent diffusion coefficients of Na in $Na_{0.44}MnO_2$ were determined to be in the range of 1.08×10^{-13}–9.15×10^{-12} cm^2 s^{-1} and 5.75×10^{-16}–2.14×10^{-14} cm^2 s^{-1} in aqueous and nonaqueous systems, respectively. The differences that they evaluated were mainly ascribed to three orders of magnitude difference in apparent diffusion coefficient along with the charge transfer resistance and the additional resistance from the formed solid-electrolyte-interphase (SEI) layer.

Since Tevar and Whitacre have introduced $Na_{0.44}MnO_2$ as cathode for ASIBs, they further prepared Na:Mn precursors with different ratios containing the α-$Na_{0.70}MnO_2$ and β-Mn_2O_3 impurity phases, and obtained the most stable electrochemical activity at a ratio of 0.6.[23] This material delivered a specific capacity of 35 mA h g^{-1} after 20 cycles at a C/1.4 rate (25 mA g^{-1}) with little capacity loss when cycled between 0.3 and 3 V (vs saturated calomel electrode (SCE)) (**Figure 5**a,b).

Driven by the limited capacity of $Na_{0.44}MnO_2$, the novel Na-rich tunnel-type positive materials with nominal composition of

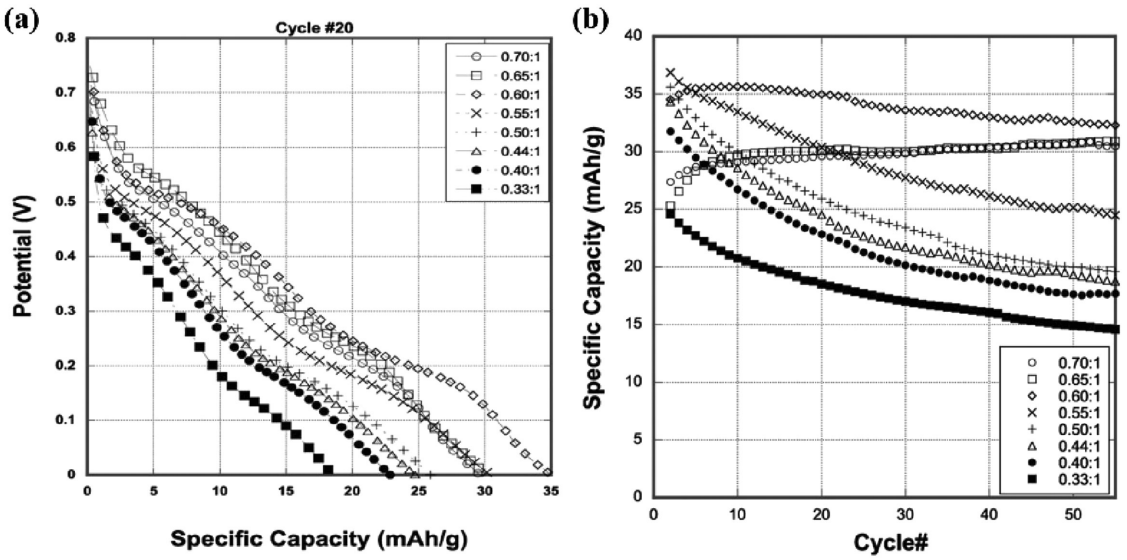

Figure 5. a) Specific capacity versus potential of the 50th discharge curve at different Na:Mn ratios. b) Specific capacities versus cycle number for all samples, showing differences in capacity losses. Reproduced with permission.[23] Copyright 2010, ECS.

$Na_{0.66}[Mn_{0.66}Ti_{0.34}]O_2$ and $Na_{0.44}[Mn_{0.66}Ti_{0.34}]O_2$ were reported by Wang et al.[24] As shown in **Figure 6**a, Na at the Na (1) site of $Na_{0.66}[Mn_{0.66}Ti_{0.34}]O_2$ is fully occupied, which is different from that in $Na_{0.44}[Mn_{0.66}Ti_{0.34}]O_2$ where the Na (1) site is not fully occupied. This Na-rich, Ti-substituted tunnel-type $Na_{0.66}[Mn_{0.66}Ti_{0.34}]O_2$ cathode material exhibited a higher reversible capacity of 76 mA h g^{-1} (at 2 C rate) in ASIBs with smaller polarization when compared to $Na_{0.44}[Mn_{0.66}Ti_{0.34}]O_2$ (Figure 6b,c). It also shows excellent cyclic performance (only small capacity decay after 300 cycles) in full cell configuration when coupled with $NaTi_2(PO_4)_3$/C (NTP/C) negative electrode, making it a promising positive electrode material for ASIBs (Figure 6d). In addition, the electrochemical Na-ion intercalation properties of $Na_{2.7}Ru_4O_9$, which is similar to $Na_{0.44}MnO_2$ structure, were investigated in 1 M Na_2SO_4 electrolyte by Kim and co-workers.[25] $Na_{2.7}Ru_4O_9$ displayed three redox peaks during the initial cycle (Figure 6e) and delivered a capacity of 28 mA h g^{-1} at 3 mA g^{-1}. However, low capacity and

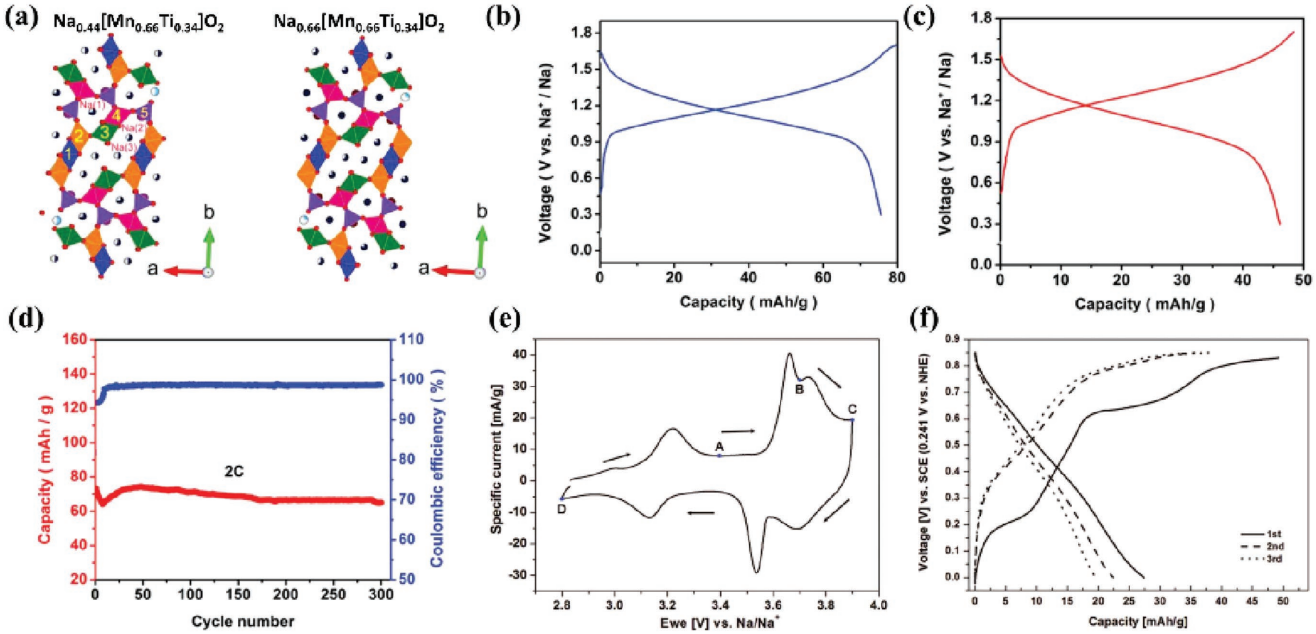

Figure 6. a) Crystal structures of $Na_{0.44}[Mn_{0.66}Ti_{0.34}]O_2$ and $Na_{0.66}[Mn_{0.66}Ti_{0.34}]O_2$. Na occupancy can be visualized by the filled dark color on each individual Na sites. The typical charge/discharge curves in the voltage range of 0.3 and 1.7 V for b) $Na_{0.44}[Mn_{0.44}Ti_{0.56}]O_2|NaTi_2(PO_4)_3$/C and c) $Na_{0.66}[Mn_{0.66}Ti_{0.34}]O_2|NaTi_2(PO_4)_3$/C full cell in aqueous electrolyte at 2 C. d) Cycling performance of $Na_{0.66}[Mn_{0.66}Ti_{0.34}]O_2|NaTi_2(PO_4)_3$/C full cell at a current rate of 2 C. Reproduced with permission.[24] Copyright 2015, Wiley. e) CV of $Na_{2.7}Ru_4O_9$ in 1 M $NaClO_4$/propylene carbonate electrolyte at a scan rate of 0.05 mV s^{-1}. f) Galvanostatic charge and discharge profiles of $Na_{2.7}Ru_4O_9$ in a 1 M Na_2SO_4 electrolyte at a current rate of 3 mA g^{-1}. Reproduced with permission.[25] Copyright 2013, ECS.

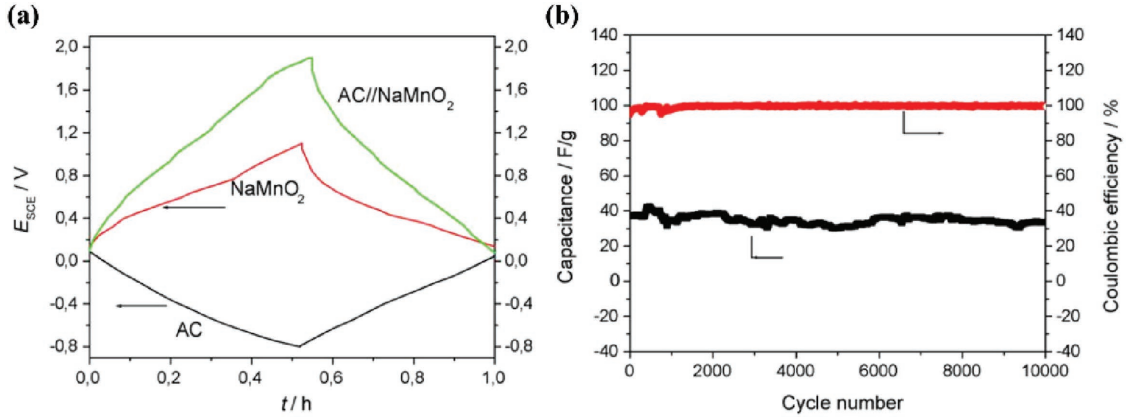

Figure 7. a) Potential–time curves of $NaMnO_2$ and AC//$NaMnO_2$ electrodes and the voltage–time profile of the asymmetric AC//$NaMnO_2$ supercapacitor at a current rate of 2 C. b) Cycling behavior of the asymmetric AC//$NaMnO_2$ supercapacitor. Reproduced with permission.[26] Copyright 2009, Elsevier.

limited cyclic stability were also observed (Figure 6f), suggesting that this material could not be an alternative for $Na_{0.44}MnO_2$ in the present form.

Apart from these materials, Qu et al. and Karikalan et al. have reported crystalline $NaMnO_2$ and 3D network of $Na_{0.21}MnO_2$, respectively, which have been applied in aqueous Na-ion hybrid supercapacitors successfully.[26,27] In Qu et al.'s work, the asymmetric AC//$NaMnO_2$ supercapacitor showed a sloping voltage profile from 0 to 1.9 V with excellent reversibility in 0.5 M Na_2SO_4 solution. Moreover, only a slight capacitance loss (<3%) after 10 000 cycles was observed at a current rate of 10 C (**Figure 7**a,b). Meanwhile, the hybrid capacitor based on $Na_{0.21}MnO_2$ cathode electrode and reduced graphene oxide (RGO) anode was designed by Karikalan et al. (**Figure 8**a).

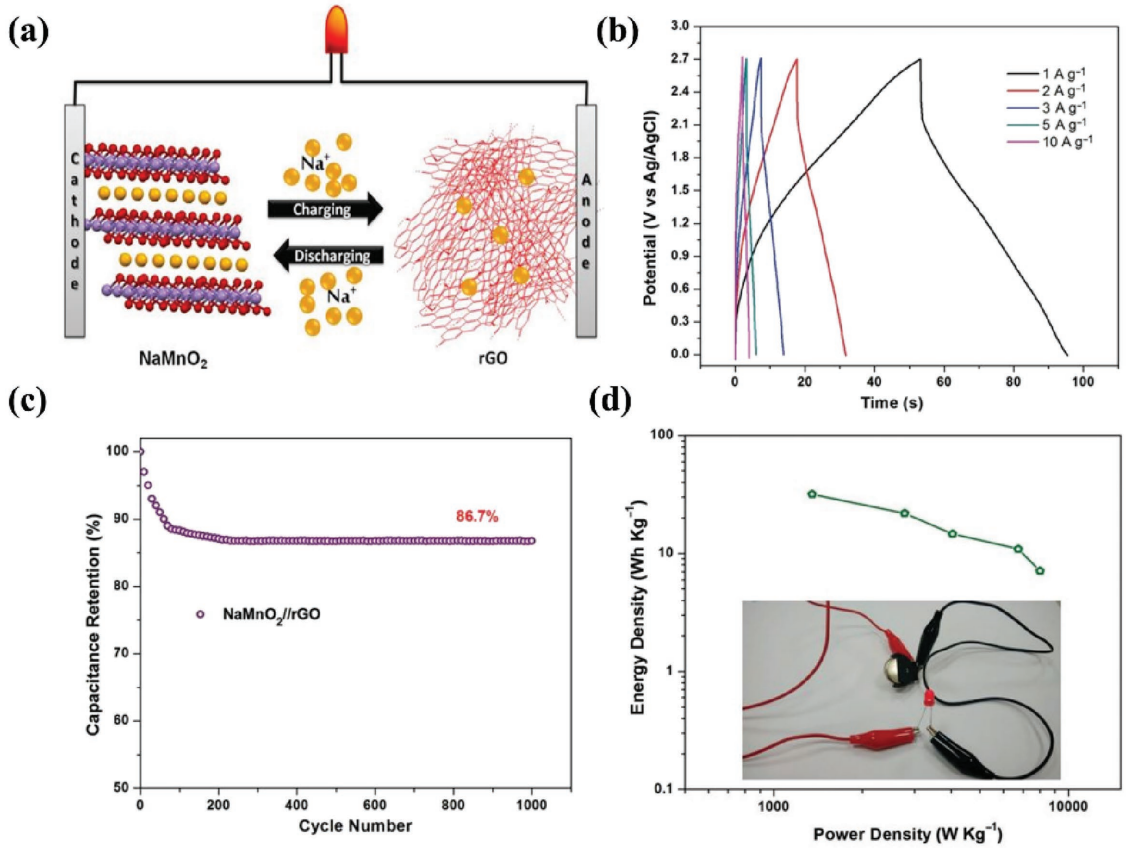

Figure 8. a) Schematic representation of Na-ion intercalation/de-intercalation for $Na_{0.21}MnO_2$//RGO capacitor. b) Galvanostatic charge/discharge profiles the asymmetric $Na_{0.21}MnO_2$//RGO capacitor conducted at a current density ranging from 1 to 10 A g^{-1}. c) Capacitance retention of the asymmetric $Na_{0.21}MnO_2$//RGO capacitor after 1000 cycles. d) The corresponding energy and power density equipped with a CR2032 coin cell. Reproduced with permission.[27] Copyright 2017, Wiley.

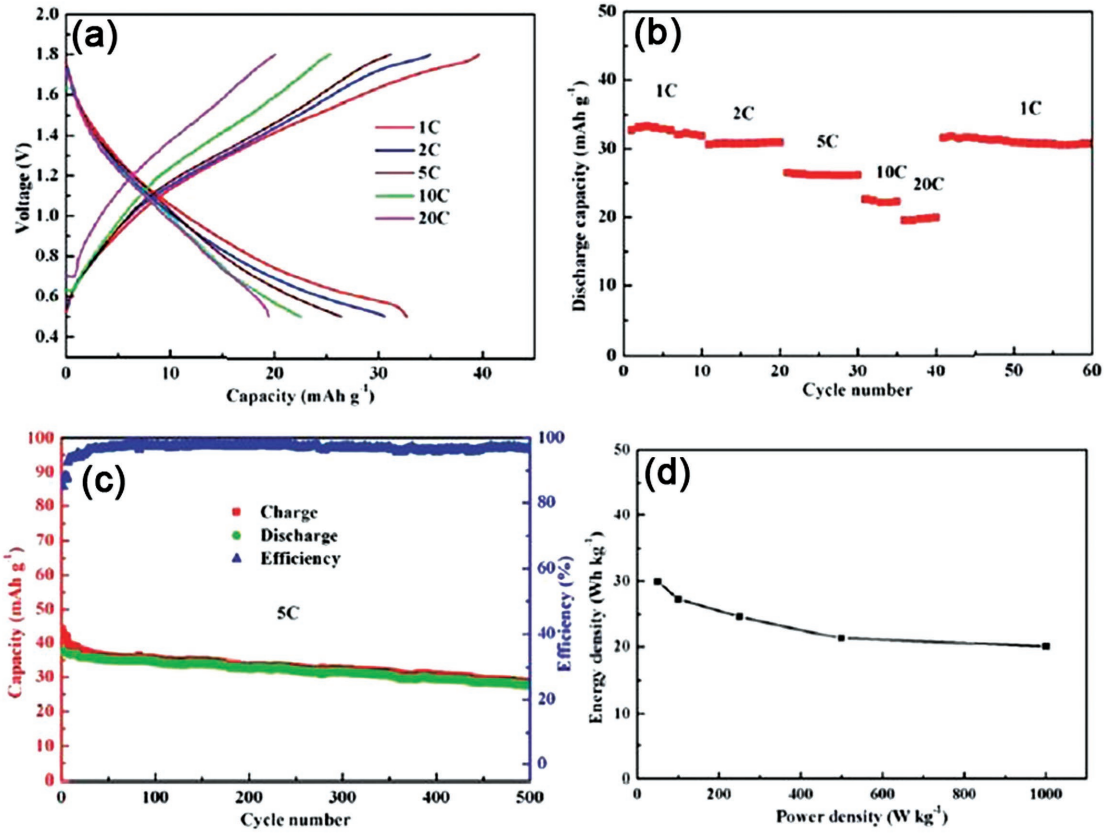

Figure 9. a) Galvanostatic curves and b) rate capability of the $NaMnO_2/NaTi_2(PO_4)_3$ full cell at different current rates. c) Cycling stability and d) Ragone plot of the full cell in aqueous electrolyte. Reproduced with permission.[28] Copyright 2015, RSC.

As shown in Figure 8b, this hybrid cell could be cycled at a large operational voltage window of 0–2.7 V and discharge up to 84.8 s at a specific current of 1 A g^{-1}. The discharge time decreased remarkably with the increasing specific current. The asymmetric capacitor achieved a capacitance retention of 86.7% after 1000 cycles in 2 M Na_2SO_4 and cellulose acetate solution. A high energy density of 31.8 Wh kg^{-1} and a power density of 1.35 kW kg^{-1} were also demonstrated to enable a 2.1 V red LED (Figure 8c,d).

In the following work, Hou et al. designed an ASIB cell using $NaMnO_2$ as the cathode and $NaTi_2(PO_4)_3/C$ composites as anode materials in 2 M CH_3COONa electrolyte. The cell could reach a wide working voltage ranged from 0.5 to 1.8 V, delivering specific discharge capacities of 33 and 23 mA h g^{-1} at 1 and 10 C rates, respectively (**Figure 9**a,b).[28] This full cell also achieved an energy density of 30 Wh kg^{-1} and 75% of the initial discharge capacity was remained after 500 cycles at the 5 C rate (Figure 9c,d).

Similarly, Zhang et al. have prepared nanowire $Na_{0.35}MnO_2$ and rod-like $Na_{0.95}MnO_2$ cathode materials for aqueous asymmetric supercapacitors using aqueous Na_2SO_4 solution electrolyte.[29] As shown in **Figure 10**a,b, the capacitance of the nanowire $Na_{0.35}MnO_2$ (157 F g^{-1}) was much higher than that of the rod-like $Na_{0.95}MnO_2$ (92 F g^{-1}). Moreover, the nanowire $Na_{0.35}MnO_2$ showed an energy density of 42.6 Wh kg^{-1} at a power density of 129.8 W kg^{-1}, which is higher than that of the rod-like $Na_{0.95}MnO_2$ electrode with an energy density of 27.3 Wh kg^{-1} at a power density of 74.8 W kg^{-1} (based on the total weight of two electrodes). These differences were ascribed to the two major reasons. First, the existence of nanowire structure can shorten the distance for the Na^+ cations' diffusion. Second, the surface area of nanowire $Na_{0.35}MnO_2$ is higher than that of rod-like $Na_{0.95}MnO_2$. Besides that, both two materials exhibited excellent cycling stability without capacitance fading up to 5000 cycles (Figure 10c,d). Liu et al. have also introduced a novel hierarchical layered $K_{0.27}MnO_2$ microflowers as cathode materials for ASIBs (**Figure 11**a).[30] When coupled with $NaTi_2(PO_4)_3$ anode, the full cell delivered a reversible capacity of 68.5 mA h g^{-1} at a current density of 0.2 A g^{-1}, and demonstrated a high capacity retention up to 100 cycles (Figure 11b,c). In 2016, they also synthesized another hollow $K_{0.27}MnO_2$ nanosphere with a specific capacity of 84.9 mA h g^{-1} at 150 mA g^{-1} in 1 M Na_2SO_4 solution (Figure 11d).[31] In the full cell configuration with hollow $K_{0.27}MnO_2$ cathode and $NaTi_2(PO_4)_3$ anode, a capacity retention of 83% was observed after 100 cycles (Figure 11e,f).

2.2. Polyanionic Compounds

Attracted by the extremely stable open framework with structural diversity and the strong inductive effect of the anions, "polyanionic" compounds have been regarded as ideal cathodes with long cycle life, enhanced rate capability, and high

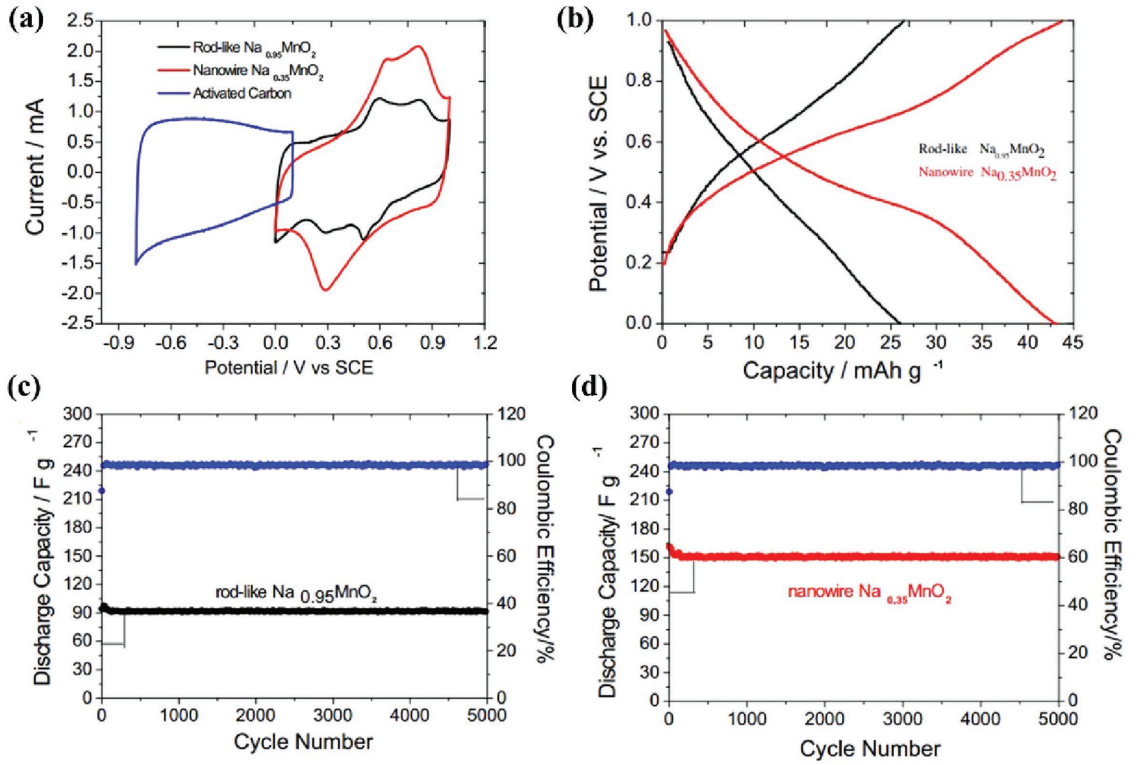

Figure 10. a) CV curves of activated carbon, the nanowire $Na_{0.35}MnO_2$, and the rod-like $Na_{0.95}MnO_2$ electrodes in 0.5 M Na_2SO_4 aqueous solution at a scan rate of 5 mV s^{-1}. b) Charge–discharge profiles of nanowire $Na_{0.35}MnO_2$ and the rod-like $Na_{0.95}MnO_2$ electrode. Cycling performance and Coulombic efficiency of c) the rod-like $Na_{0.95}MnO_2$ and d) nanowire $Na_{0.35}MnO_2$. Reproduced with permission.[29] Copyright 2014, Elsevier.

safety.[32,33] Since the new phases of polyanionic compounds, $Na_4M_3(PO_4)_2P_2O_7$ (M = Fe, Mn, Co, and Ni), have been synthesized by Sanz et al, succeeding researcher have further tailored these materials to use in organic sodium-ion battery.[34–36] Among these phosphate-based materials, $Na_4Fe_3(PO_4)_2P_2O_7$ displays two low voltage plateaus at ≈2.9 and ≈3.2 V versus Na^+/Na, whereas the reversibility and cyclability of this material are not satisfactory, as reported by Kang and

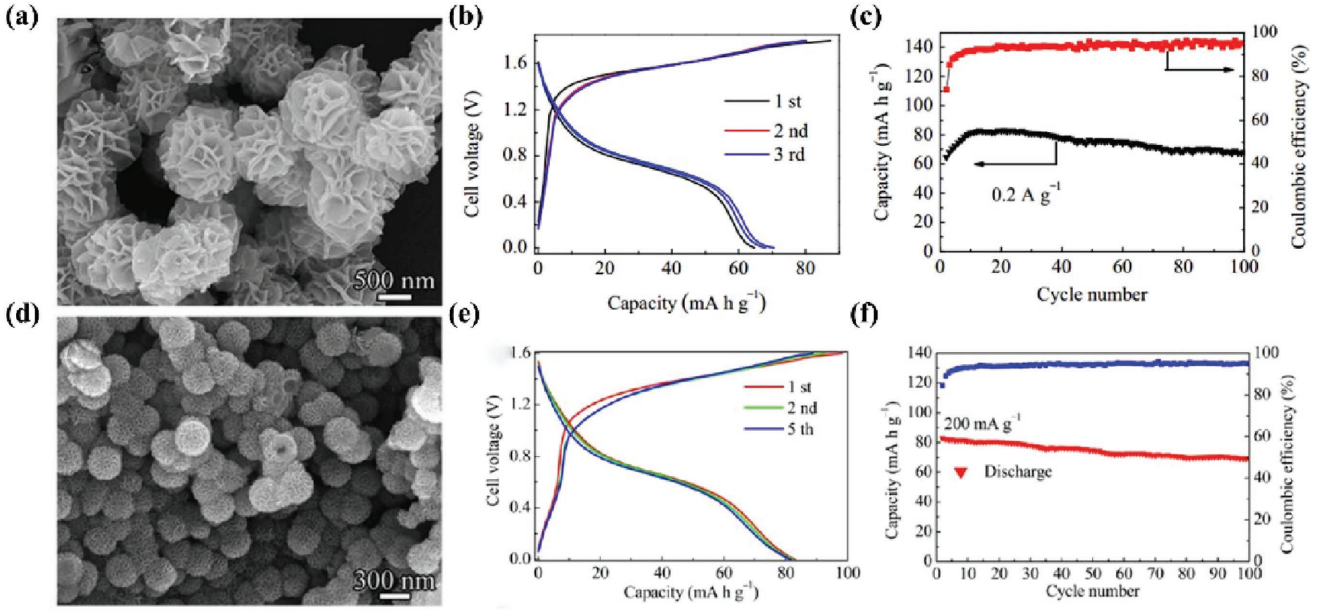

Figure 11. a) scanning electrode microscopy (SEM) images of layered $K_{0.27}MnO_2$ microflowers, b) charge/discharge profiles, and c) cycle stability of $K_{0.27}MnO_2$ microflowers at a current density of 0.2 A g^{-1}. Reproduced with permission.[30] Copyright 2014, Elsevier. d) SEM images of hollow $K_{0.27}MnO_2$ nanospheres. e) Charge/discharge profiles and f) cycle stability of hollow $K_{0.27}MnO_2$ nanospheres at a current density of 200 mA g^{-1}. Reproduced with permission.[31] Copyright 2016, ACS.

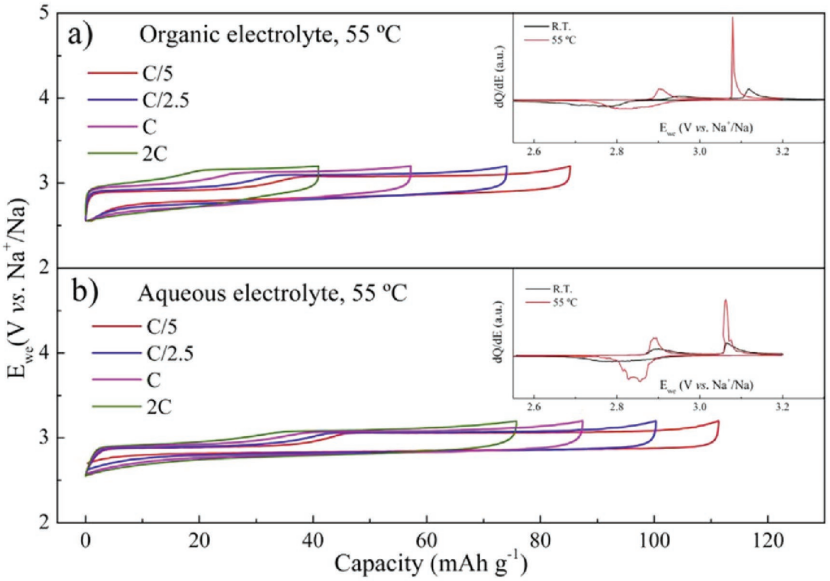

Figure 12. Charge/discharge profiles of $NaFePO_4$ at different rates for a) an organic cell and b) an aqueous cell cycled between 2.55 and 3.2 V versus Na^+/Na at 55 °C. Inset: d*Q*/d*E* plots for a C/5 rate at room temperature and 55 °C. Reproduced with permission.[40] Copyright 2015, Elsevier.

co-workers.[37] Transition metal alteration from Fe to Ni, Co, and Mn increases the cell voltage from 3.2 V versus Na^+/Na to high voltage for this $Na_4M_3(PO_4)_2P_2O_7$, which can lead to the oxygen evolution when this has been used in aqueous solution.[36,38] Therefore, whether these high-voltage materials could be considered as electrodes in ASIBs has yet to be studied further. As one of the important polyanionic compounds, amorphous-phase $NaFePO_4$ could exhibit a high discharge capacity of ≈150 mA h g^{-1}, which has reported by Ali et al.[39] However, it operates at a low working potential (≈2.4 V) with a sloping discharge profile, which may render it inappropriate for ASIBs use. Subsequently, Fernández-Ropero et al. have studied the electrochemical performance of $NaFePO_4$ as cathode material in aqueous and nonaqueous electrolytes under various temperatures and voltage windows.[40] As shown in **Figure 12**, the polarization in both electrolytes was reduced with a more realistic operation temperature (55 °C). More significantly, polarization decreased in aqueous media. Indeed, the capacity at C/5 reached 110 and almost 87 mA h g^{-1} at 1 C in aqueous electrolyte, which was superior to the obtained value in nonaqueous electrolyte. By tuning the voltage window properly, the capacity retention was significantly improved, indicating that this material is a potential candidate for cathode in ASIBs.

In addition, pioneer researchers found that some polyanionic compounds can be used as cathode for ASIBs. Song et al. have prepared the NASICON-type $Na_3V_2(PO_4)_3$ (NVP) cathode with large tunnels to accommodate the large Na ions for lattice perturbation-free intercalation/de-intercalation processes. They investigated the electrochemical activity of NVP in 1 M Li_2SO_4, Na_2SO_4, and K_2SO_4 electrolytes.[41] As shown in **Figure 13**a, one pair of redox peaks are observed from the cyclic voltammogram (CV) curve, corresponding to the Na-ion insertion/extraction. The change of current at various scan rates indicates a diffusion-controlled process of the NVP electrode in Na_2SO_4 solution. In a three-electrode system, the NVP electrode exhibited charge/discharge capacitances of 209, 173, 136, and 74 F g^{-1} at 8.5, 17, 42.7, and 85 C, respectively (Figure 13b). However, the unsatisfactory Coulombic efficiency (≈80%) and capacitance retention (≈32% in the 30th cycle) were important issues that should be addressed (Figure 13c). Recently, Zhang et al. developed a new ASIB based on all NASICON-structured electrodes with $NaTi_2(PO_4)_3$ anode and $Na_3V_2(PO_4)_3$ cathode in the Na_2SO_4 electrolyte.[42] Such a battery fulfilled the theoretical working window of aqueous electrolyte and exhibited a high output voltage of 1.2 V (Figure 13e). The first charge and discharge capacities of NVP were 103 and 73 mA h g^{-1} at 2 A g^{-1}, respectively, exceeding the previous reported value of the same material in aqueous electrolyte (Figure 13d). Even at a high current density of 10 A g^{-1}, the battery delivered a discharge capacity of 58 mA h g^{-1}. However, the cell has shown unfavorable cycling stability. At a high current of 10 A g^{-1}, only 50% of the initial capacity was remained after 50 cycles (Figure 13f).

It has been widely known that many vanadium compounds suffer from the dissolution of V species, leading to large irreversible charge capacity and poor cycling stability in ASIBs. Recently, some researchers have explored novel Na–vanadium phosphate stabilized by another substituted atom while their original open 3D framework structure remained unchanged.[43–45] For example, by replacing one V^{3+} cation from $Na_3V_2(PO_4)_3$ with Ti^{4+}, Wang et al. have synthesized NASICON-structured $Na_2VTi(PO_4)_3$ material for the first time through a high-safety and low-cost route.[45] The $Na_2VTi(PO_4)_3$ material has been used as the cathode and anode electrodes with the redox couples of V^{4+}/V^{3+} and Ti^{4+}/Ti^{3+}, respectively, as shown in **Figure 14**a,b. The redox potentials of vanadium and titanium present in NASICON-structured compounds are stable within the electrochemical potential window of water. Therefore, they can be applied as either anode or cathode without the electrochemical decomposition of water. The symmetric full cell fabrication based on the bifunctional $Na_2VTi(PO_4)_3$ electrode displays a well-defined voltage plateau at ≈1.2 V, a charge capacity of 62 mA g^{-1} at a rate of 1 C, and an impressive cycling stability with a capacity retention of 70% for 1000 cycles at 10 C (Figure 14c,d).

Another typical NASICON-based full cell was reported by Gao and Goodenough.[44] They have prepared $Na_3MnTi(PO_4)_3$, which can also be used as both anode and cathode in aqueous electrolytes, by introducing Mn^{2+} and Ti^{4+} to substitute V^{3+} cation (**Figure 15**a). The quasisymmetric reactions are based on the redox couples of Mn^{3+}/Mn^{2+} and Ti^{4+}/Ti^{3+} (as anode, reversibly inserting one Na ion). It has been shown that the charge/discharge profiles are centered around 1.4 V without apparent polarization during subsequent cycles, and a reversible capacity of 57.9 mA h g^{-1} was achieved at 0.5 C (Figure 15b). The rate capability of the symmetric cell was also evaluated at different charge/discharge rates from 0.5 to 10 C. Reversible capacities of 56.5 and 46.7 mA h g^{-1}

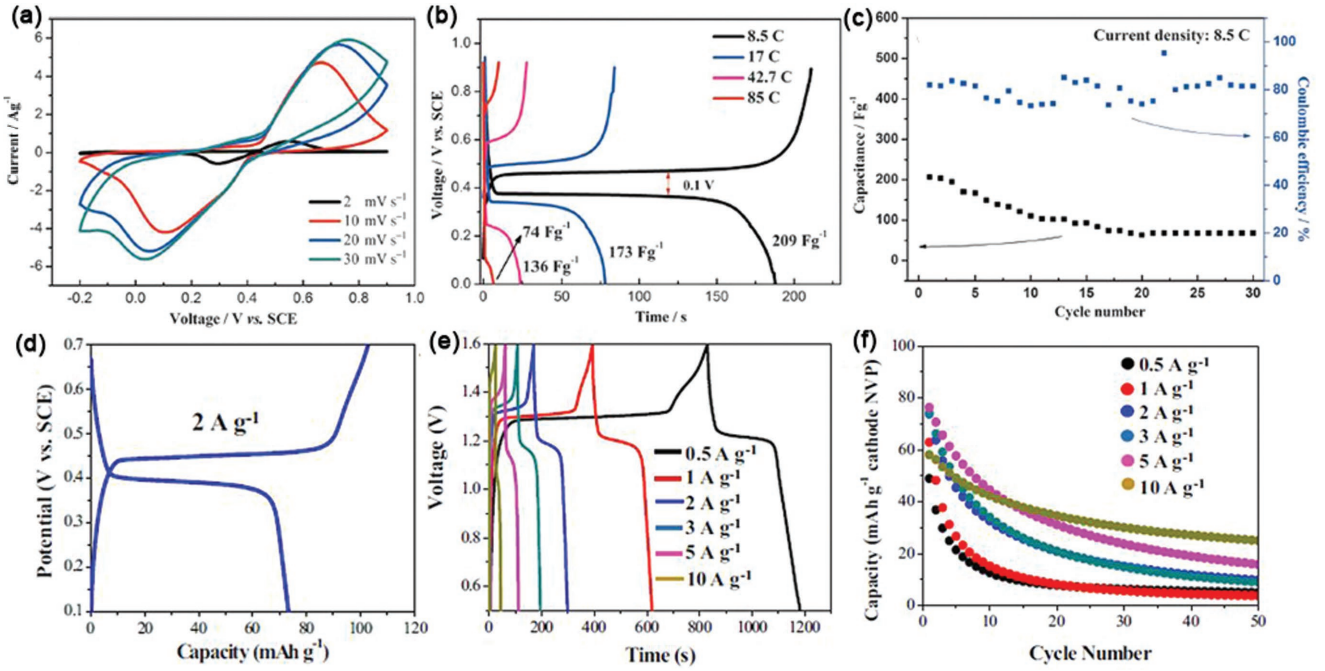

Figure 13. a) CV curves obtained at different scan rates in 1 M Na_2SO_4 solution. b) Charge/discharge profiles and c) cycle performance and Coulombic efficiency of $Na_3V_2(PO_4)_3$ in 1 M Na_2SO_4 aqueous electrolyte measured at a 8.5 C rate. Reproduced with permission.[41] Copyright 2014, Wiley. d) The first charge/discharge profiles of $Na_3V_2(PO_4)_3$ in 1 M Na_2SO_4 aqueous half-cell. e) Charge–discharge curves of the NTP/NVP full cell at various current densities. f) Cycling performance of NTP/NVP full cell at various current densities. Reproduced with permission.[42] Copyright 2016, Elsevier.

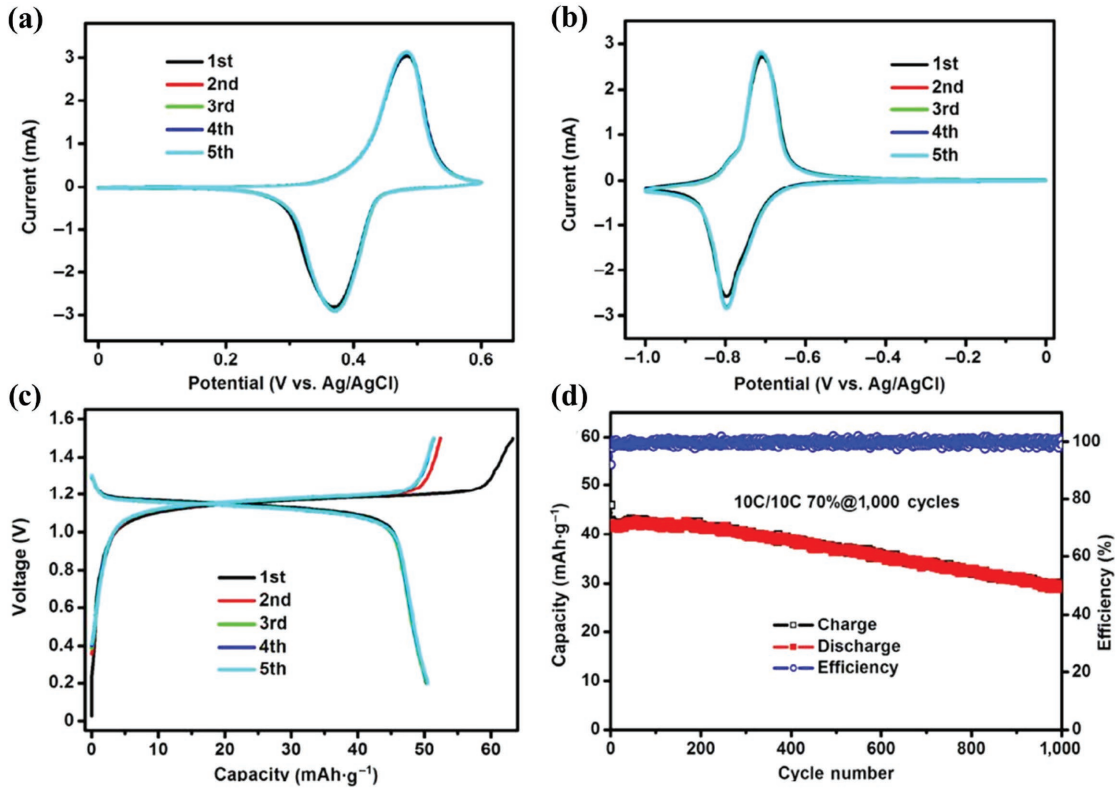

Figure 14. CV curves of the $Na_2VTi(PO_4)_3$ electrode as a) anode and b) cathode at a scan rate of 0.5 mV s^{-1} in 1 M Na_2SO_4 solution. c) Typical charge/discharge profiles of the aqueous full cell in the voltage range of 0.2–1.5 V at a rate of 1 C. d) The cycling performance and corresponding Coulombic efficiency over 1000 cycles at a rate of 10 C. Reproduced with permission.[45] Copyright 2017, Springer.

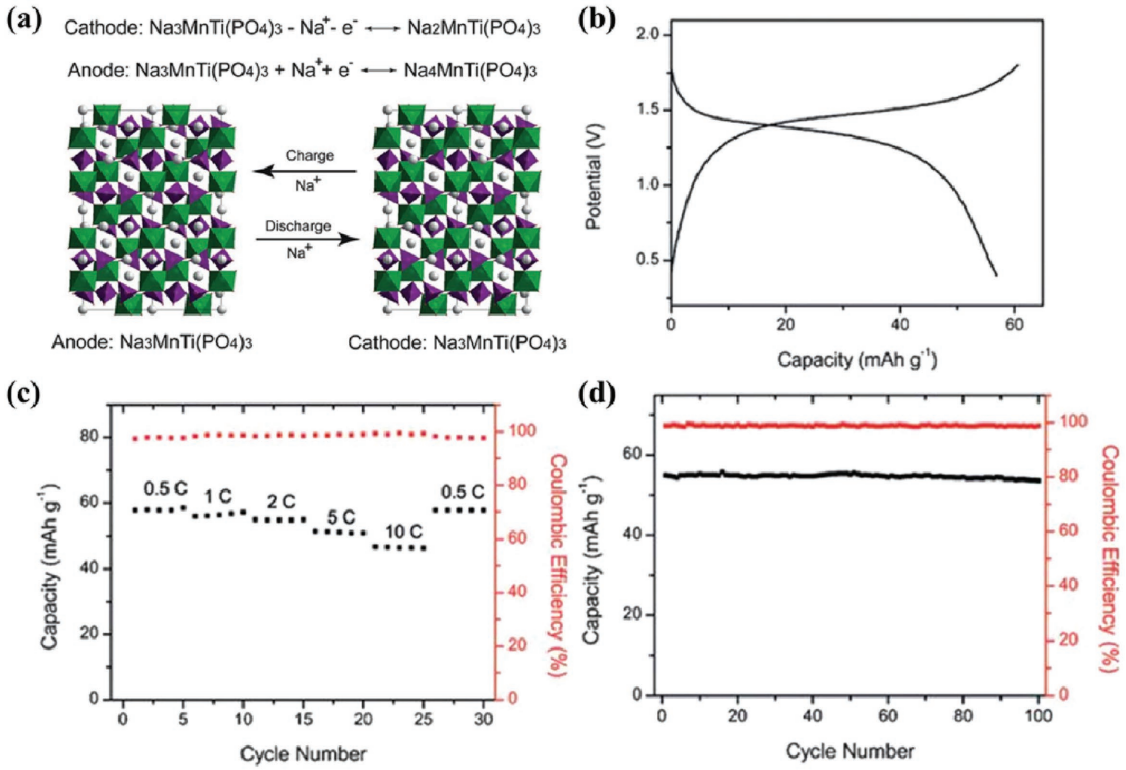

Figure 15. a) Schematic illustration of the aqueous symmetric sodium-ion battery with NASICON-structured $Na_3MnTi(PO_4)_3$ anode and cathode. b) The charge/discharge profiles of aqueous $Na_3MnTi(PO_4)_3/Na_3MnTi(PO_4)_3$ battery tested between 0.4 and 1.8 V at a rate of 0.5 C. c) Rate performance of symmetric sodium-ion battery cycled at various current rates from 0.5 to 10 C. d) Cycling performance of the symmetric sodium-ion battery at the current rate of 2 C after 100 cycles. Reproduced with permission.[44] Copyright 2016, Wiley.

have been obtained at 1 and 10 C rates, respectively (Figure 15c). Importantly, about 98% of the initial capacity was retained after 100 cycles at 1 C with a Coulombic efficiency of more than 99% (Figure 15d). These results confirmed that high-safety, long-life, and low-cost stationary battery systems can be obtained using a single active material in the aqueous electrolyte.

Additionally, NASICON-type $Na_3V_2O_2(PO_4)_2F$ nanocubes and multiwalled carbon nanotubes' (MWCNT) composites has been reported by Kumar et al., and utilized as an Na-ion cathode in both nonaqueous and aqueous electrolytes.[46] Owing to the extreme electronegativity of F, the $Na_3V_2O_2(PO_4)_2F$–MWCNT composite showed higher redox potentials of reversible Na^+ ion extraction and insertion in 2% vinylene carbonate (VC) contained 10 M $NaClO_4$ aqueous electrolytes. An initial discharge capacity of 44 mA h g^{-1} was attained and 81% of the initial capacity was retained after 50 cycles at 1 C rate (**Figure 16**a).

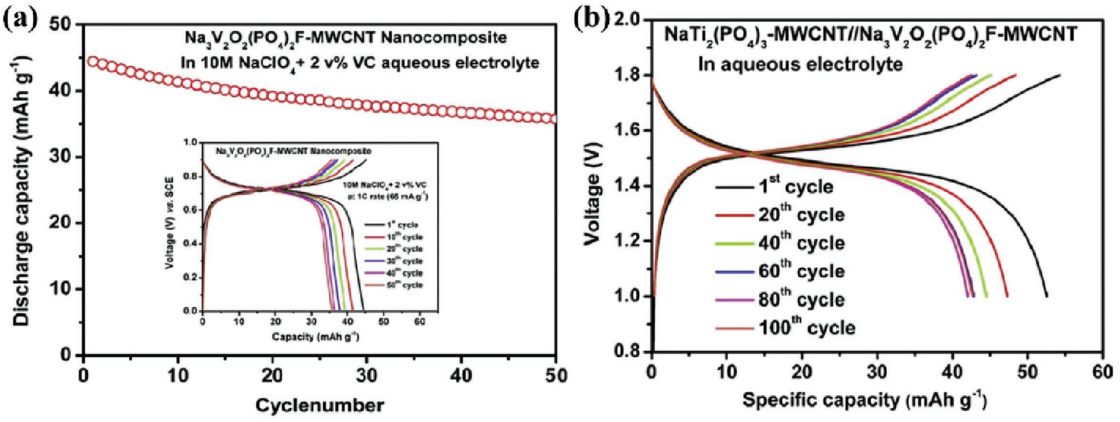

Figure 16. a) Cycling performance at 1 C rate for the $Na_3V_2O_2(PO_4)_2F$–MWCNT nanocomposite in 10 M $NaClO_4$ + 2% VC electrolyte solution. The inset figure shows the charge–discharge curves at 1 C rate. b) Charge–discharge curves for the $NaTi_2(PO_4)_3$–MWCNT//$Na_3V_2O_2(PO_4)_2F$–MWCNT full cell in aqueous electrolytes. Reproduced with permission.[46] Copyright 2016, Elsevier.

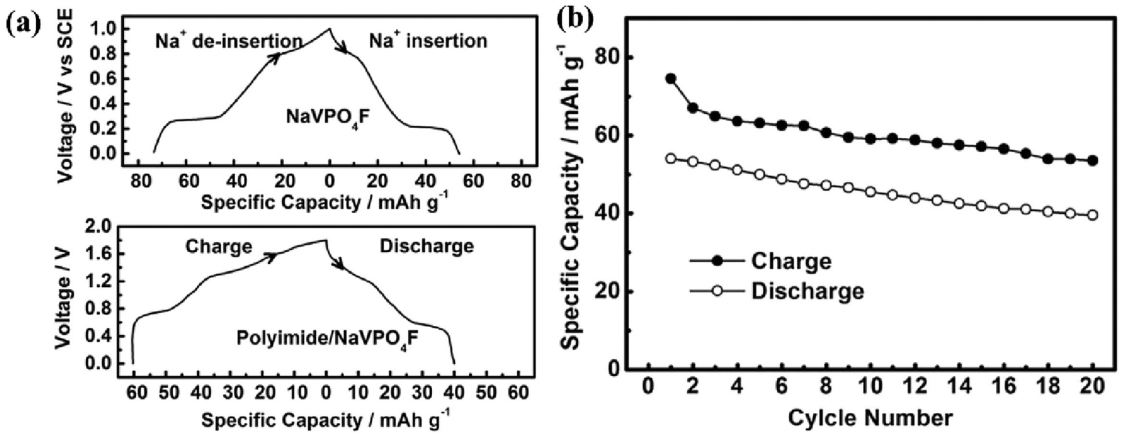

Figure 17. a) Charge/discharge curves in the first cycle of $NaVPO_4F$ electrode and polyimide/$NaVPO_4F$ full cell in 5 M $NaNO_3$ aqueous electrolyte. b) The cycling profiles of $NaVPO_4F$ in 5 M $NaNO_3$ solution at a current density of 50 mA g^{-1}. Reproduced with permission.[47] Copyright 2014, Elsevier.

The $Na_3V_2O_2(PO_4)_2F$–MWCNT cathode was then coupled with $NaTi_2(PO_4)_3$–MWCNT anode to assemble an asymmetric Na-ion full cell. The integrated full cell, which operated in a voltage range of 1.0–1.8 V, delivered a high working voltage of 1.5 V, and a discharge capacity of 42 mA h g^{-1} after 100 cycles at 1 C rate (80% of the initial capacity) with an excellent average Coulombic efficiency of 99% (Figure 14b).

$NaVPO_4F$, another NASICON-type cathode material, was reported by Qin et al.[47] Two pairs of redox peaks at 0.26/0.20 and 0.79/0.77 versus SCE in 5 M $NaNO_3$ aqueous solution were observed, which are associated with the two different insertion/extraction processes (**Figure 17**a). However, the capacity of polyimide/$NaVPO_4F$ full cell decreased from 40 mA h g^{-1} in the 1st cycle to about 30 mA h g^{-1} in the 20th cycle, indicating its poor cycling stability (Figure 17b). Iron-based pyrophosphate compound, $Na_2FeP_2O_7$, cathode material for ASIBs has also been reported by Jung et al.[48] The galvanostatic discharge profiles at 1 and 5 C in nonaqueous and aqueous electrolytes are displayed in **Figure 18**a. Obviously, the capacity changes at higher rate (5 C) and lower rate (1 C) in aqueous electrolyte were much smaller than that of nonaqueous electrolyte. The higher rate capability in aqueous electrolytes is ascribed to the higher ionic diffusivity. Cycling performance of over 300 cycles in the potential range of –0.2 to +0.7 V (vs SCE) was also obtained at both 1 and 5 C rates in an aqueous system (Figure 18b).

2.3. Prussian Blue Analogs

Apart from the aforementioned materials, another important class of cathode materials for ASIBs is Prussian blue analogs (PBAs). They have recently received attention as cathode materials for rechargeable nonaqueous Li-ion batterries due to several promising properties. First, they have appropriate open framework crystal structures, $A_xPR(CN)_6$, which accounts for large interval space that can accommodate the alkali metal ion with rapid insertion/extraction reaction. Moreover, previous studies have found that thin-film Prussian blue analogs have electrochemical activities in Na ion and other alkali-metal-ion-based aqueous electrolytes.[49–51] Recently, Cui and co-workers have synthesized a series of Prussian blue derivatives, which show excellent Na-ion storage behavior in ASIBs.[52] For instance, nickel hexacyanoferrate (NiHCF) was prepared by a coprecipitation method that ensured consistent reaction conditions. The electrochemical reaction of NiHCF is described by the following expression: $ANiFe^{3+}(CN)_6 + A^+ + e^- = A_2NiFe^{2+}(CN)_6$, where A^+ is an

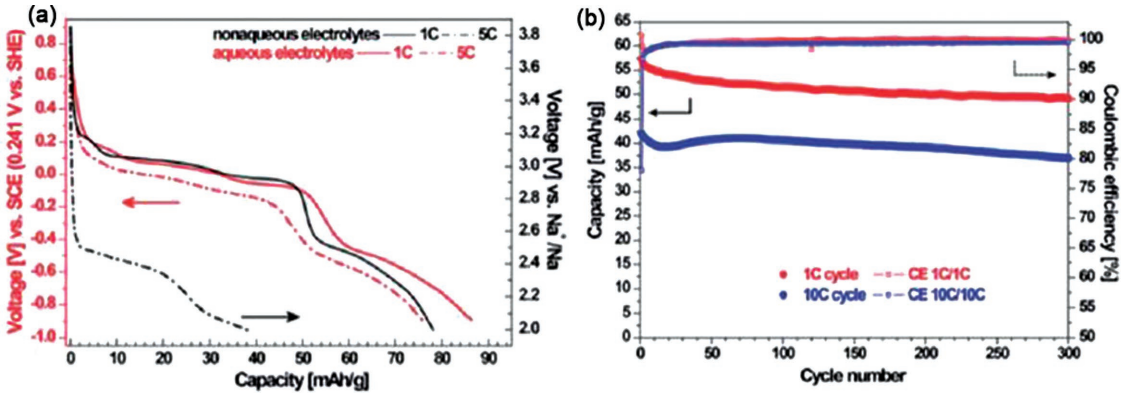

Figure 18. a) Galvanostatic discharge curves of $Na_2FeP_2O_7$ electrode at a rate of 1 and 5 C in nonaqueous and aqueous electrolytes. b) The corresponding capacity retention at 1 and 10 C in aqueous electrolyte. Reproduced with permission.[48] Copyright 2014, RSC.

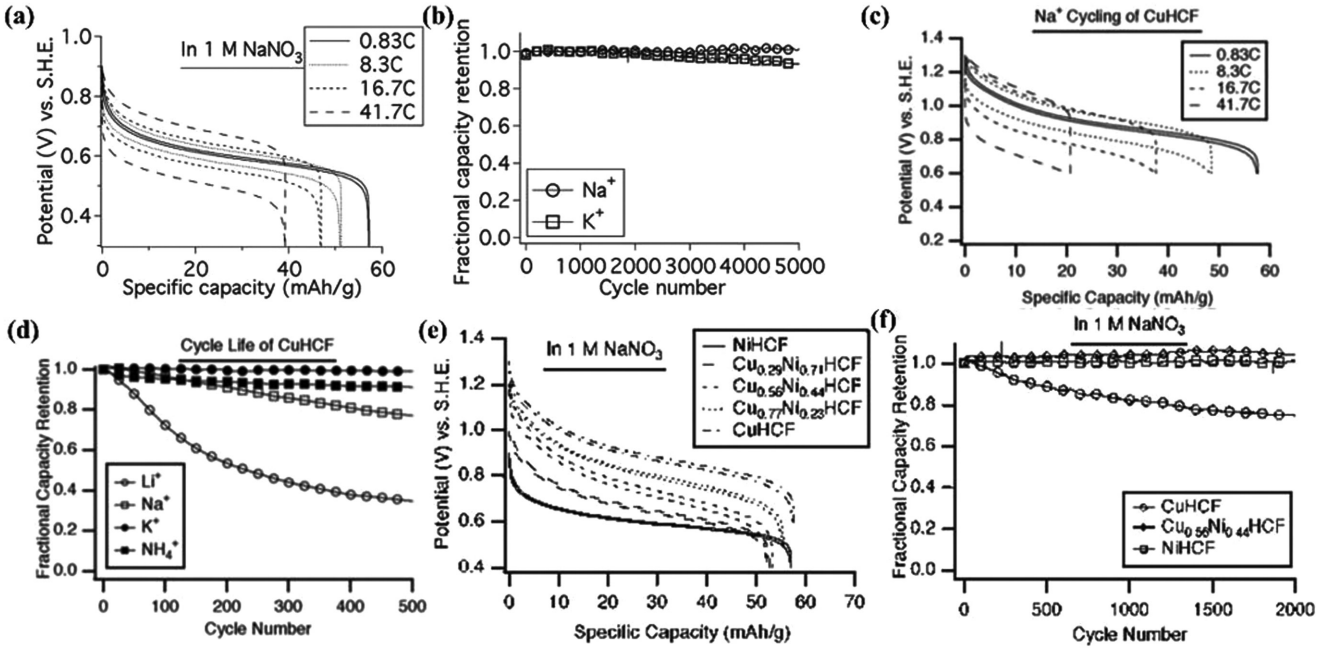

Figure 19. a) The potential profiles of NiHCF during galvanostatic charge–discharge in 1 M $NaNO_3$ electrolyte. b) The cycle performance of NiHCF during galvanostatic cycling of Na^+ and K^+ at the 8.3 C rate. Reproduced with permission.[52] Copyright 2011, ACS. c) Charge/discharge profiles of CuHCF at different rates in aqueous electrolyte. d) The cycle life of CuHCF during cycling of Li^+, Na^+, K^+, and NH_4^+ solution. Reproduced with permission.[53] Copyright 2012, ECS. e) Potential profiles of different ratios of CuNiHCF during galvanostatic charge/discharge in 1 M $NaNO_3$. f) $Cu_{0.56}Ni_{0.44}HCF$ cycling data from 2000 cycles at 0.5 A g^{-1} in 1 M $NaNO_3$. Reproduced with permission.[54] Copyright 2012, ACS.

alkali ion, such as Na or potassium. It was found that NiHCF reacts with Na at 0.59 V versus standard hydrogen electrode (SHE) in aqueous $NaNO_3$ solution. A specific capacity of 59 mA h g^{-1} was delivered at a 0.83 C rate, the rate performance that was also evaluated by Na cycling of NiHCF, shows 86.5% and 67% capacity retentions at rates of 8.3 and 41.7 C, respectively (**Figure 19**a). More importantly, NiHCF showed superior cycling stability with zero capacity loss after 5000 cycles at 8.3 C rate (Figure 19b). In contrast to PBA thin films, the behavior of bulk CuHCF and NiHCF electrodes were subsequently investigated in aqueous electrolytes containing Li^+, Na^+, K^+, and NH_4^+ ions.[53] The PBAs with the coordination of different metal elements exhibit various redox potentials to be used as a cathode. Figure 19c shows that CuHCF electrode displayed a redox potential of 0.9 V versus SHE in aqueous $NaNO_3$ electrolyte, obviously higher than that on NiHCF electrode (0.5 V). A similar capacity of ≈60 mA h g^{-1} was observed, which indicates that the CuHCF electrode can achieve higher energy density in ASIBs. Although inferior cycling stability was observed compared to NiHCF, the CuHCF electrode exhibited higher rate capability at 8.3 C and retained 77% of its initial capacity after 500 cycles (Figure 19d). In their other work, nanosized CuNiHCF was further synthesized using a precipitation method.[54] By tuning the ratio of Ni to Cu in the hybrid material, the various redox potentials of CuNiHCF from 0. 6 to 1.0 V could be achieved in 1 M $NaNO_3$ aqueous electrolyte (Figure 19e). The long-term cycling performance in Figure 19f shows that NiHCF and $Cu_{0.56}Ni_{0.44}HCF$ display no capacity loss after 2000 cycles at 0.5 A g^{-1}, while CuHCF loses 25% of its initial capacity.

Jiang et al. have also introduced graphene-modified copper hexacyanoferrate (CuHCF/Gr) as a cathode material for aqueous Li_2SO_4/Na_2SO_4-mixed-ion electrolyte battery. The voltage plateaus of CuHCF/Gr in mixed electrolytes were more similar to the ones in Na_2SO_4 solution.[55] The discharge capacities of CuHCF/Gr in 0.1 M Li_2SO_4 + 0.4 M Na_2SO_4, and 0.25 M Li_2SO_4 + 0.25 M Na_2SO_4 at 60 C were found to be 86.7% and 85.5%, respectively, higher than the one in 0.5 M Li_2SO_4 (83.7%). The higher capacity indicates that the introduction of Na^+ into Li_2SO_4 electrolytes is beneficial to the high rate capability of CuHCF/Gr (**Figure 20**a,b). In addition, Kim et al. have paired disodium naphthalenedimide (SNDI) anode, a Prussian blue derivatives, with $KCo_{0.5}Cu_{0.5}Fe(CN)_6$ cathode to form a hybrid aqueous Na full cell.[56] As observed in **Figure 21**a, the full cell shows an average potential of ≈1.1 V and delivers 34 mA h g^{-1} at 20 C charging/10 C discharging. It also exhibits stable cycling performance by preserving 88% of the initial capacity after 100 cycle (Figure 21b).

In a recent work, high-quality iron hexacyanoferrate nanocubes (HQ-PB NCs), reported by Cai et al., were investigated as a cathode electrode material for ASIBs.[57] Two couples of well-separated redox peaks are observed in the CV curve in aqueous 1 M Na_2SO_4 electrolyte, involving the reversible insertion/extraction reactions of two Na^+ ions, as shown in **Figure 22**a. Discharge capacities of 126.1, 115.4, 106.7, 100.0, 93.9, 88.2, and 83.3 mA h g^{-1} were obtained at different current densities of 0.25, 0.5, 1, 1.5, 2, 2.5, and 3 A g^{-1}, respectively (Figure 22b). Impressively, as displayed in Figure 22c, the HQ-PB NCs exhibited a high discharge capacity of 99.0 mA h g^{-1} after 200 cycles at a high current density of 1.25 A g^{-1} (about 96.3% retention).

Most recently, a new kind of PBAs consisting of vanadium and iron ions (V/Fe PBAs) was designed as a cathode material

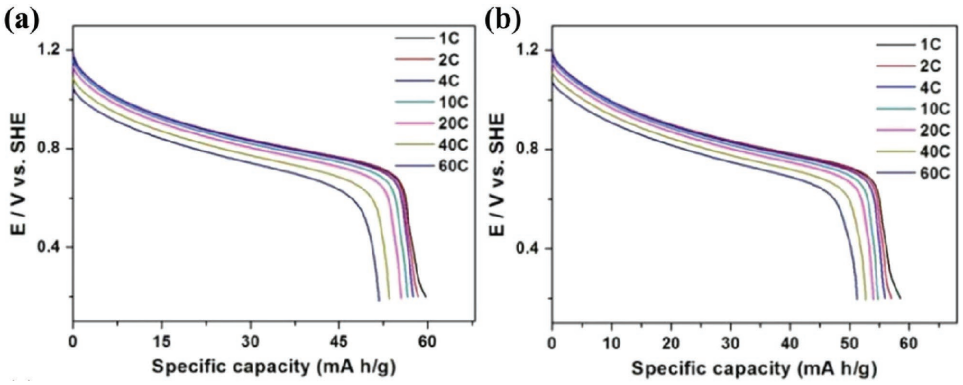

Figure 20. Rate capabilities of CuHCF in aqueous a) 0.1 M Li_2SO_4 + 0.4 M Na_2SO_4 and b) 0.25 M Li_2SO_4 + 0.25 M Na_2SO_4 solution. Reproduced with permission.[55] Copyright 2017, RSC.

for ASIBs.[58] Taking advantage of the multielectron redox reactions of V and Fe ions, Lee et al. have found that V/Fe PBAs delivered improved discharge capacity of 90 mA h g^{-1} at a current density of 0.11 A g^{-1} (1.2 C) compared to previously reported PBAs including Cu/Fe and Ni/Fe (**Figure 23**a). As noted in the CV curves (Figure 23b), the V/Fe PBA cathodes react electrochemically through three redox processes, with middle reaction potentials (E_{mid}, defined as ($E_{oxidation}$ + $E_{reduction}$)/2) of 0.54, 0.90, and 1.08 V. Moreover, the V/Fe PBAs exhibited a high cycling stability and Coulombic efficiency, retaining a capacity of ≈55 mA h g^{-1} at the end of 250th cycle (Figure 23c).

Although the above Ni- and Cu-based Prussian blue displayed a considerable rate capability and stability performance, they could not be directly considered as the cathode materials to assemble full ASIBs since these compounds are typical Na-free cathode materials. In this regard, Wu et al. first tried to use Na-rich material as cathode for aqueous Na_2SO_4 electrolyte.[59] A distinct charge and discharge profile with well-defined voltage plateaus at 0.4–0.6 V and a reversible discharge capacity of 65 mA h g^{-1} at a current density of 65 mA g^{-1} were observed in **Figure 24**a. In addition, the cycling stability of the $Na_2NiFe(CN)_6$ electrode was shown in Figure 24b. This electrode can be very well cycled up to 500 cycles at 5 C rate with only slight capacity decay. In their other work, they have synthesized Na-rich copper hexacyanoferrate (II) $Na_2CuFe(CN)_6$ as a high potential cathode and $NaTi_2(PO_4)_3$ as an anode to assemble an ASIB.[60] They found that, under a similar discharge capacity of 59 mA h g^{-1}, the $Na_2CuFe(CN)_6$ electrode displayed charge/discharge plateaus at ≈0.61 V (vs Ag/AgCl), obviously higher than that of $Na_2NiFe(CN)_6$, implying an effective enhancement in the working voltage of this ASIB (Figure 24c). Figure 24d shows that the discharge capacity decreases slightly from 57 to 53 mA h g^{-1} over 500 cycles at the 5 C rate, corresponding to 93% capacity retention and a 100% Coulombic efficiency. Similarly, the high-quality and vacancy-free $Na_xCoFe(CN)_6$ nanocrystals were investigated in the aqueous electrochemical Na-storage reaction. This material could deliver a high capacity of 130 mA h g^{-1} at a current density of 130 mA g^{-1}, as shown in Figure 24e. The NaCoHCF nanocrystals also demonstrated high capability at 20 C and superior capacity retention of 90% over 800 cycles (Figure 24f).[61]

In addition, they have synthesized Na-rich $Na_{1.33}Fe[Fe(CN)_6]_{0.82}$ derived from the low-defect $FeFe(CN)_6$ nanocrystals.[62] The reversible capacity of the $Na_{1.33}Fe[Fe(CN)_6]_{0.82}$ cathode sustained stable at 122 mA h g^{-1}, which was in agreement with the capacity of Na-deficient $FeFe(CN)_6$ nanocrystals, and a cycling stability with 93% capacity retention over 40 cycles was also observed, as shown in **Figure 25**a,b. Fernández-Ropero et al. have studied the electrochemical properties of Na Prussian blue, $Na_{1-x}Fe^{III}_{1+(x/3)}[Fe^{II}(CN)_6]\cdot yH_2O$ (x = 0.25).[63] Rate capability tests (Figure 25c) revealed that, as compared to the capacity obtained in organic electrolyte, the $NaFe_2(CN)_6$ PBA was able to deliver 65 mA h g^{-1} of enhanced capacity at 0.2 C, and retained

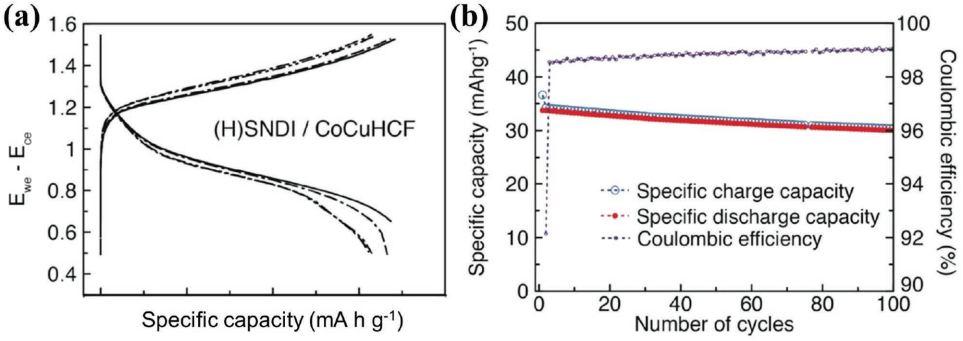

Figure 21. a) The galvanostatic charge/discharge profiles, b) cycling performance, and Coulombic efficiencies of SNDI/CoCuHCF aqueous full cells. Reproduced with permission.[56] Copyright 2014, Wiley.

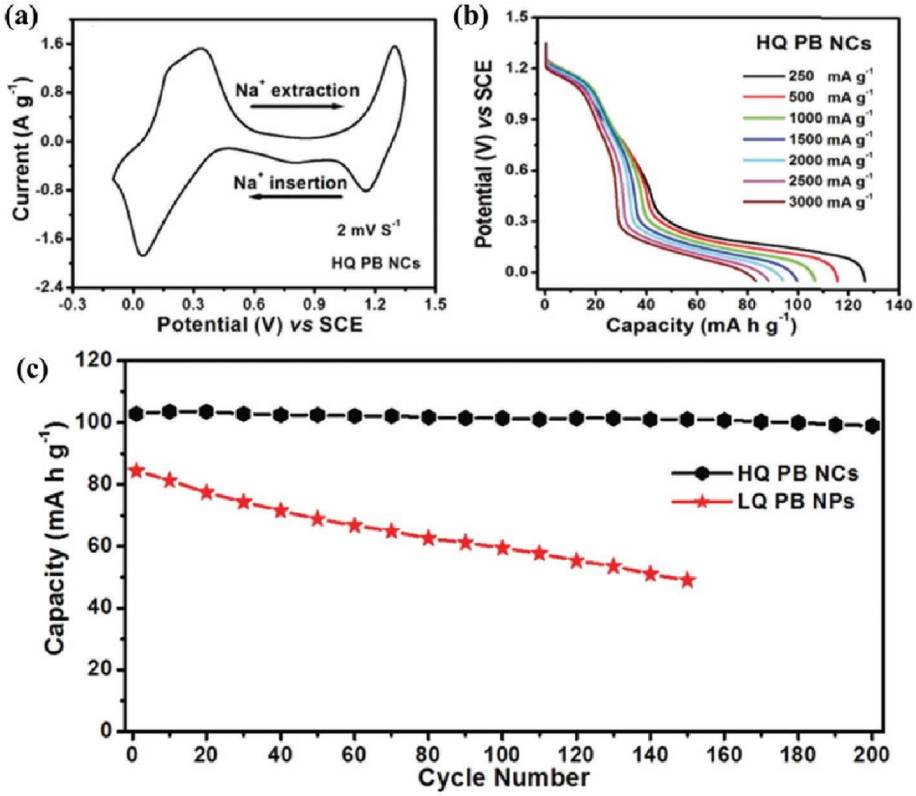

Figure 22. a) CV curve of the HQ–PB NCs recorded at a scan rate of 2 mV s^{-1} in aqueous electrolyte. b) Discharge curve of HQ–PB NCs' electrode at different current densities. c) The cycling performance of the HQ–PB NCs and low quality prussian blue NPs at a high current density of 1.25 A g^{-1}. Reproduced with permission.[57] Copyright 2017, RSC.

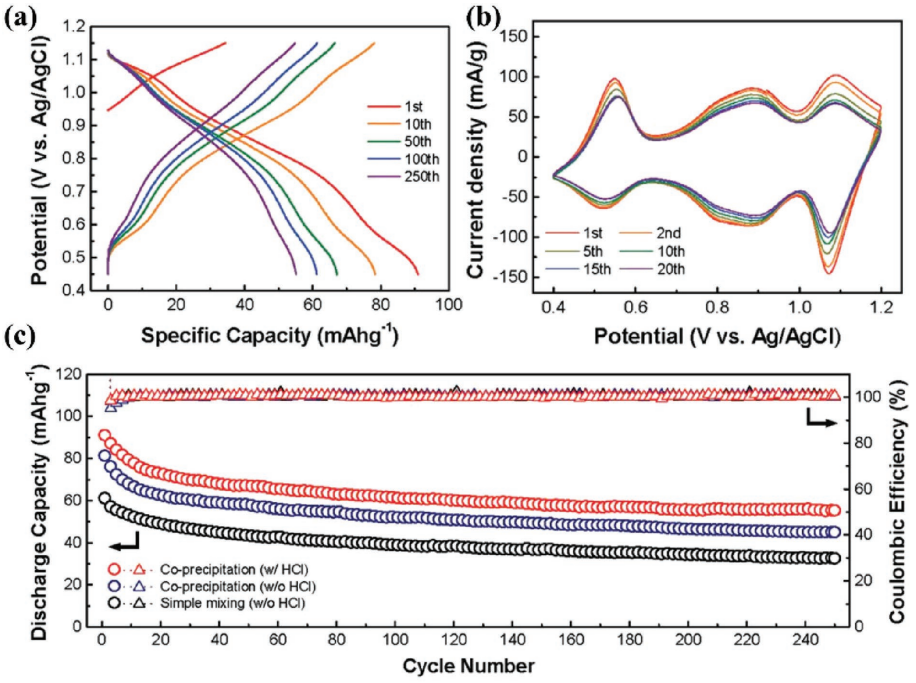

Figure 23. a) Charge/discharge profiles of the Ni/Fe PBAs based on coprecipitation (with HCl), evolving over 250 cycles at 0.11 A g^{-1}. b) CV curves of Ni/Fe PBAs within a potential range of 0.4–1.2 V versus Ag/AgCl for the initial 20 cycles. c) Discharge capacity and Coulombic efficiency depending on the different synthetic procedures. Reproduced with permission.[58] Copyright 2017, Wiley.

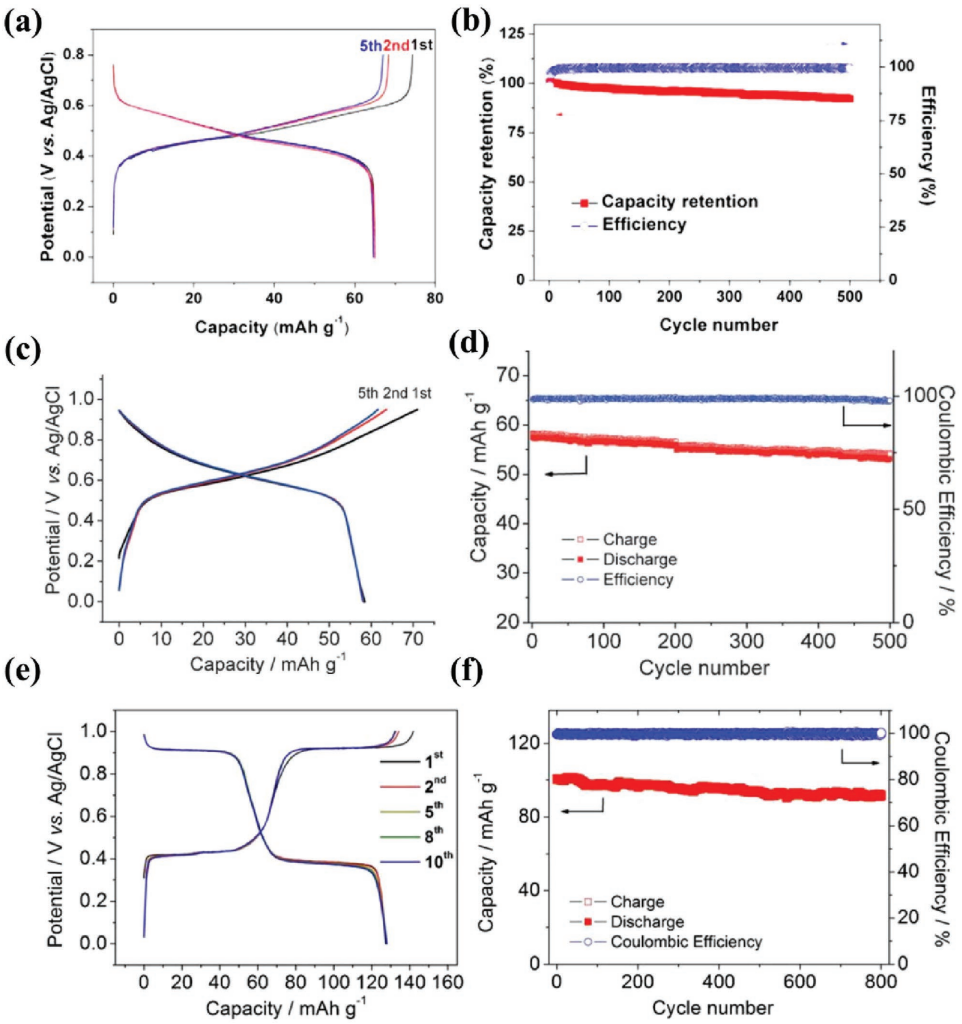

Figure 24. a) Charge/discharge profiles at 65 mA g^{-1} and b) cycling stability at a constant current of 5 C of $Na_2NiFe(CN)_6$ cathode electrode. Reproduced with permission.[59] Copyright 2013, Elsevier. c) Charge/discharge profiles at 65 mA g^{-1} and d) cycling stability at a constant current of 5 C of $Na_2CuFe(CN)_6$ cathode electrode. Reproduced with permission.[60] Copyright 2014, Wiley. e) Charge/discharge profiles at 130 mA g^{-1} and f) cycling stability at a constant current of 5 C of NaCoHCF cathode. Reproduced with permission.[61] Copyright 2015, Wiley.

a capacity of 26 mA h g^{-1} at 10 C in 1 M Na_2SO_4 aqueous solution. As shown in Figure 25d, 61 mA h g^{-1} of the reversible capacity was obtained at 0.2 C which is similar to previously reported PBAs, and 84% of the initial capacity could be retained after 200 cycles at a current rate of 1 C.

Another Na-rich vanadium-based PBA, namely $Na_2VO_x[Fe(CN)_6]$, thin film (VHCF) was recently proposed by Paulitsch et al. for application in ASIBs.[64] The obtained VHCFs demonstrated a very positive half-charge potential ($\Delta E_{1/2} \approx 0.91$ V vs Ag/AgCl) with nearly the same specific capacity recorded at high 30 C in 1 M $LiNO_3$, 3 M $NaNO_3$, and 3 M KNO_3 electrolytes in the presence of 3.6 M H_2SO_4 (**Figure 26**a). By depositing $Na_2Ni[Fe(CN)_6]$ thin protective layer on VHCF films, this VHCF/NiHCF composite exhibited a higher Na-ion intercalation/de-intercalation potential (0.78/0.71 V) in the acidic media when compared with the pure $Na_2VO_x[Fe(CN)_6]$ films (Figure 26b). On the basis of Na storage of low $Fe(CN)_6$ defects, an aqueous rechargeable Na–Zn battery with NaFe-PB as a cathode and a zinc anode was first developed by Wang et al.[65] As shown in Figure 26c, the two sets of reversible processes located at 0 V versus Zn/Zn^{2+} from the reversible deposition/dissolution of zinc were observed. Another two pairs of redox peaks are also observed at ≈1.0–1.5 V versus Zn/Zn^{2+}, which are derived from reversible conversion between Fe^{3+} and Fe^{2+} accompanied by the insertion/extraction of Na^+ in the NaFe-PB material. Figure 26d displayed that the full cell was operated in a suitable voltage range 0.9–1.6 V under a current density of 100 mA g^{-1}, and exhibited a discharge capacity of 78.5 mA h g^{-1} for NaFe-PB in aqueous Na_2SO_4 solution. When assembled with the Zn anode, the long cycling performance of the aqueous full cell was evaluated at a high current density of 300 mA g^{-1} and the corresponding capacity retention was about 80% after 1000 cycles (Figure 26e).

2.4. Other Na-Based Compounds

In addition to the above-mentioned cathode materials, some researchers have also attempted to explore other compounds

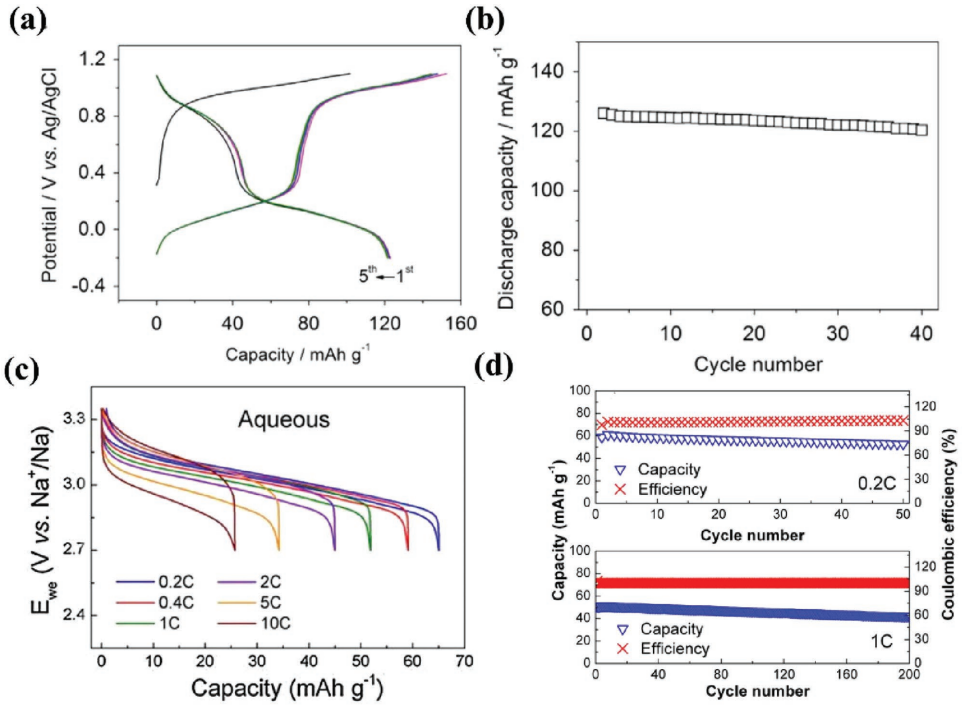

Figure 25. a) Charge/discharge profiles at 65 mA g^{-1} and b) cycling stability at a constant current of 5 C after 50 cycles on the $Na_{1.33}Fe[Fe(CN)_6]_{0.82}$ electrode. Reproduced with permission.[62] Copyright 2015, Elsevier. c) Charge/discharge profiles of $NaFe_2(CN)_6$ PB at different rates in aqueous electrolyte. d) Discharge specific capacity and Coulombic efficiency displayed by two aqueous cells cycled at 0.2 and 1 C. Reproduced with permission.[63] Copyright 2016, Elsevier.

as cathode materials in ASIBs. For instance, Minakshi et al. have proposed the maricite of $NaMn_{1/3}Ni_{1/3}Co_{1/3}PO_4$ cathode coupled with AC anode for stationary renewable energy storage applications using an aqueous NaOH electrolyte.[66] The aqueous hybrid capacitor studied by charge–discharge cycling in the potential range of 0.4–1.8 V at 0.5 A g^{-1} exhibited a specific discharge capacitance of 45 F g^{-1} which is stable over 1000 cycles (**Figure 27**a). P_2-type-layered $Na_{2/3}Ni_{1/4}Mn_{3/4}O_2$, reported by Yu et al., has also been utilized as a cathode material in aqueous hybrid Na^+/Li^+ electrolyte by adopting activated carbon as the counter electrode.[67] It was found that the $Na_{2/3}Ni_{1/4}Mn_{3/4}O_2$ electrode could deliver a desirable discharge capacity of 54 mA h g^{-1}, when the Na^+/Li^+ ratio in mixed Na^+ and Li^+ aqueous solution was 2:2 (Figure 27b). Recently, our group present a novel aqueous battery system that depends the redox of I^-/I^{3-} couple in liquid cathode and the reversible enolization in polyimide anode, accompanied by Na^+ (or Li^+) diffusion between cathode and anode through an Na^+/Li^+ exchange polymer membrane.[68] As illustrated in **Figure 28**a, I^- ions are oxidized into I^{3-} ions during charging, and, simultaneously, Na ions (or Li ions) in liquid cathode diffuse across the ion exchange separator to react with polyimide anode to form Na_x–polyimide or (Li_x–polyimide) through an "enolization process" [$(C{=}O)_n \rightarrow (C{-}O{-}Na/Li)_n$]. The rate capability of full aqueous Na-ion battery was evaluated (Figure 28b). It delivered a high capacity of 95 mA h g^{-1} at a high current density of 20 A g^{-1}, maintained an impressive capacity of 28 mA h g^{-1} even at an extremely high current density of 100 A g^{-1}. Most surprisingly, the full cell can be stably cycled over 50 000 times with a capacity retention of 70%, which is close to that of the aqueous Li-ion battery mentioned earlier (Figure 28c).

3. Anode Materials

3.1. NASICON-Type $NaTi_2(PO_4)_3$

Although numerous titanium-based materials have been extensively studied as anode materials for rechargeable SIBs in organic electrolyte, only NASICON-type $NaTi_2(PO_4)_3$ is reported as a potential anode of ASIBs. A number of related publications have also come out in the past few years. Park et al. first investigated reversible electrochemical Na insertion into NASICON-type $NaTi_2(PO_4)_3$ in aqueous and nonaqueous electrolytes.[69] In the case of $NaTi_2(PO_4)_3$, 2 moles of Na ions are reversibly inserted based on a Ti^{3+}/Ti^{4+} redox couple, producing the discharge state of $Na_3Ti_2(PO_4)_3$. A large reversible capacity of 133 mA h g^{-1}, corresponding to 93% of the theoretical capacity, was obtained, with a flat operating voltage of 2.1 V which is appropriate for Na^+ insertion without the evolution of H_2. Notably, the charge/discharge polarization of the $NaTi_2(PO_4)_3$ electrode in aqueous electrolyte was considerably smaller than in nonaqueous electrolyte especially at a large current density of 2.0 mA cm^{-2}, which is ascribed to the smaller impedance and the low viscosity of the aqueous electrolyte (**Figure 29**). The capacity fading of the $NaTi_2(PO_4)_3$ in aqueous lithium-ion batteries has been examined by our group. We have found that

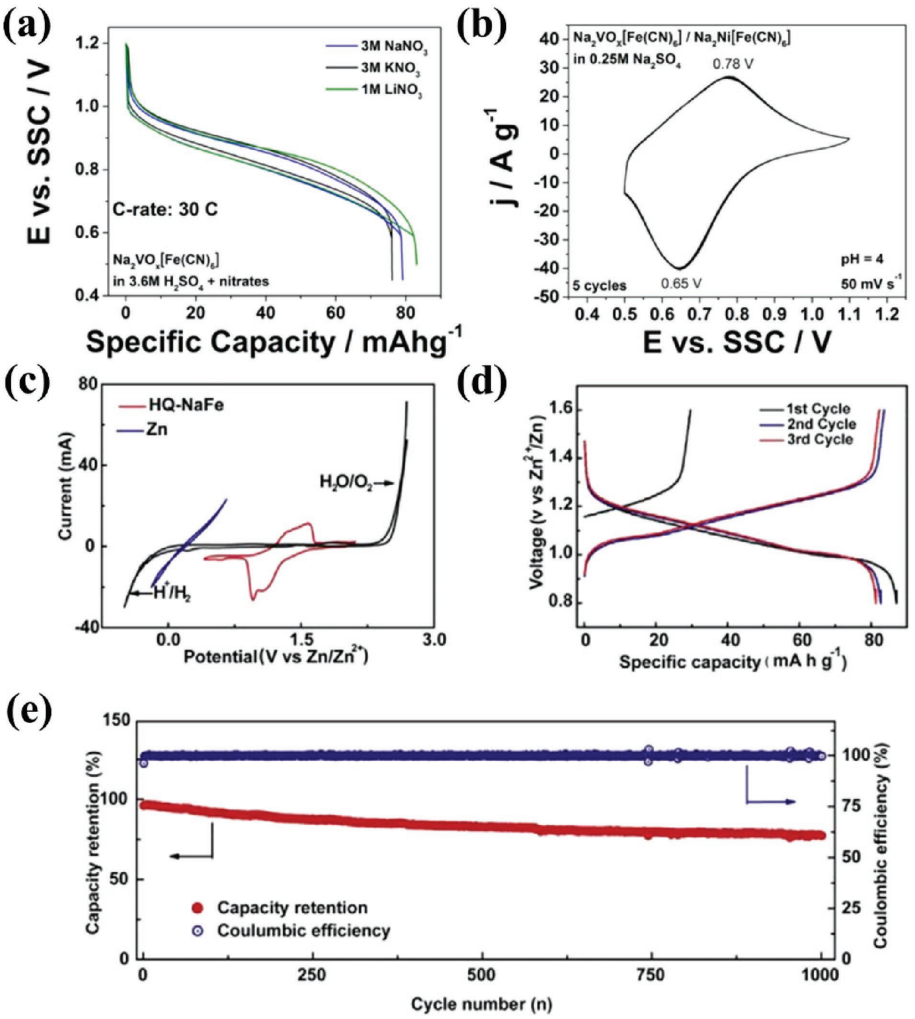

Figure 26. a) Galvanostatic charge and discharge curves at the 30 C rate for the $Na_2VO_x[Fe(CN)_6]$ films in 1 M $LiNO_3$, 3 M $NaNO_3$, and 3 M KNO_3 with 3.6 M H_2SO_4 electrolytes. b) CV curves of "VHCF/NiHCF" protected thin film in 0.25 M Na_2SO_4 in the potential range of 0.5–1.1 V. Reproduced with permission.[64] Copyright 2017, ACS. c) CV curves of NaFe–PB and Zn foil in aqueous Na_2SO_4 electrolyte measured at a scanning rate of 1 mV s^{-1}. d) Galvanostatic discharge/charge voltage profiles of aqueous Na/Zn full cell under a current density of 100 mA g^{-1}. e) Long cycling performance of aqueous Na/Zn full cell under a current density of 300 mA g^{-1}. Reproduced with permission.[65] Copyright 2017, Elsevier.

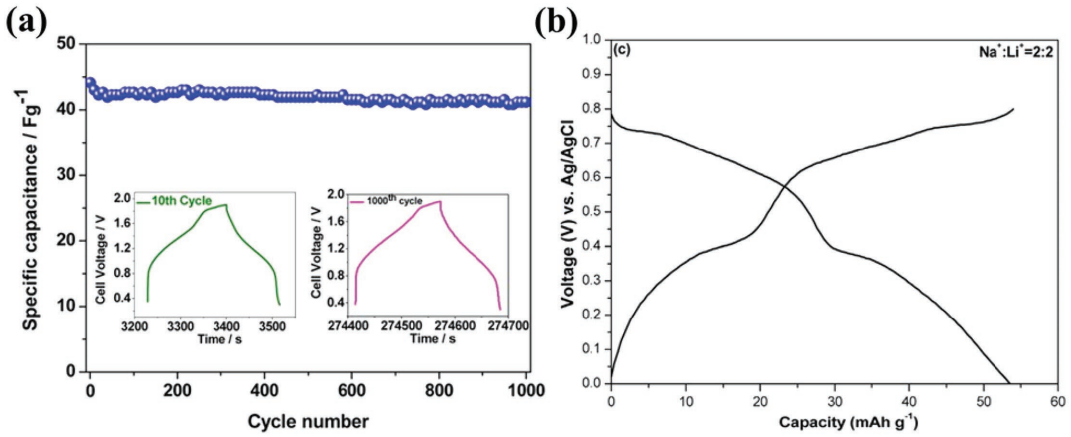

Figure 27. a) Specific capacitance versus cycle life of $NaMn_{1/3}Ni_{1/3}Co_{1/3}PO_4$||AC hybrid capacitor cycled 1000 times, the inset show 10th and 1000th cycles of the hybrid cell. Reproduced with permission.[66] Copyright 2013, ACS. b) The charge/discharge profiles of $Na_{2/3}Ni_{1/4}Mn_{3/4}O_2$ in 1 M aqueous electrolyte with 2:2 molar ratio of Na^+:Li^+. Reproduced with permission.[67] Copyright 2017, Elsevier.

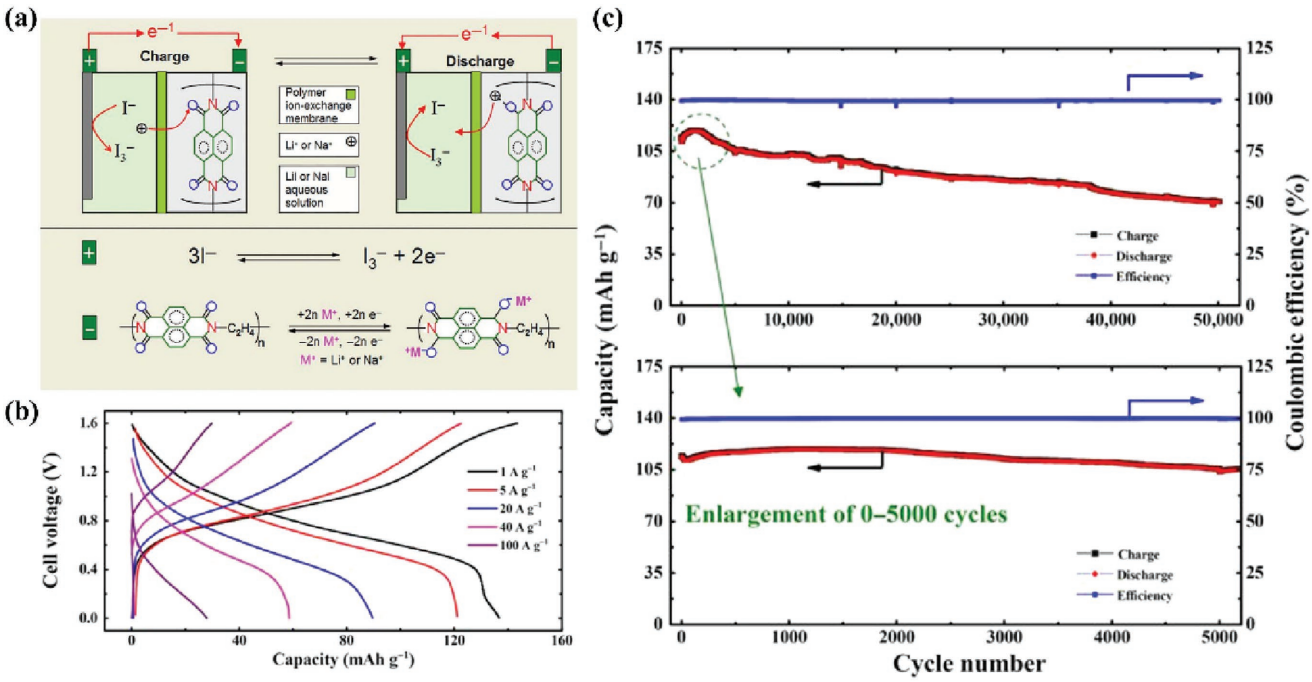

Figure 28. a) Schematic illustration of cell structure and electrode reactions. b) The charge–discharge profiles of aqueous Na-ion battery based on solid poly-1,4,5,8-naphthalenetetracarboxylic dianhydride anode and liquid I^-/I^{3-} cathode at different current rates. c) The superior long cycle life of this aqueous Na-ion battery based on the mass of anode material. Reproduced with permission.[68] Copyright 2016, AAAS.

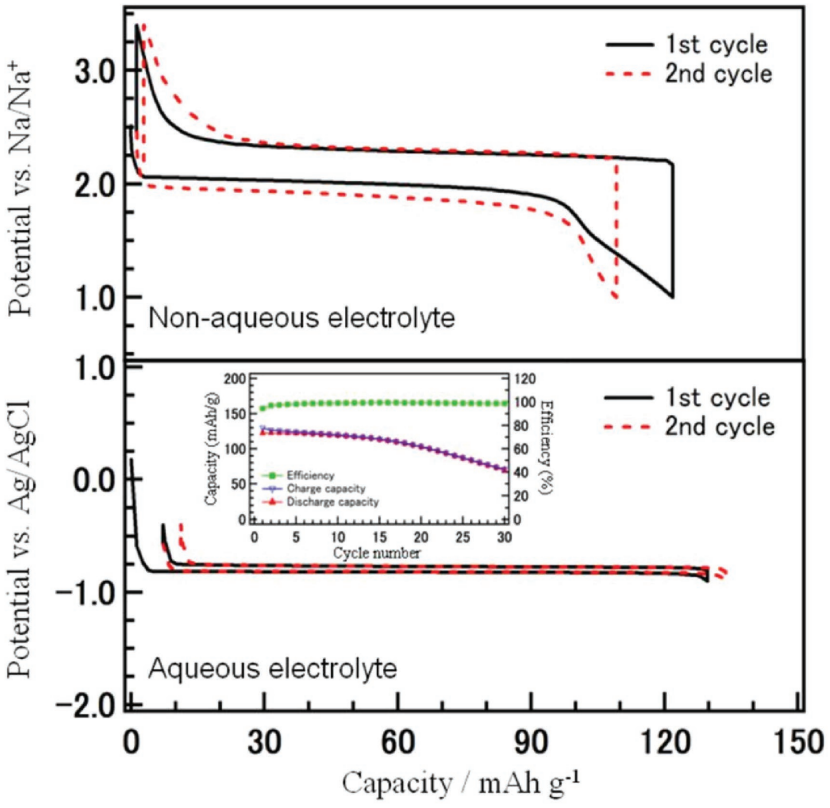

Figure 29. Charge/discharge profiles of $NaTi_2(PO_4)_3$//Na in nonaqueous electrolyte and $NaTi_2(PO_4)_3$//Zn in aqueous electrolyte at a rate of 2.0 mA cm^{-2}. The inset represents the dependence of the capacity on the cycle number for carbon thermally treated $NaTi_2(PO_4)_3$. Reproduced with permission.[69] Copyright 2011, ECS.

Li-ion intercalated anode materials at the discharged state would react with water and O_2, regardless of the pH value of the electrolyte.[70] Therefore, the pure $NaTi_2(PO_4)_3$ suffered from the poor cycling stability and conductivity in aqueous electrolyte similar to the $LiTi_2(PO_4)_3$ material.

In the development highly stable electrode materials, carbon coating is the most widely adopted technique to improve the electronic conductivity and surface characteristic. For example, graphite-coated $NaTi_2(PO_4)_3$ with additional carbon nanotubes (CNTs) was prepared by Wu et al., and the composite material displayed desirable electrochemical performances. The first cycle discharge specific capacities were 130 and 75 mA h g^{-1} at 0.1 and 2 C rates, respectively (**Figure 30**a).[71] Furthermore, a capacity retention of 86% was demonstrated under continuous charge/discharge at 1 C rate for 100 cycles, demonstrating their good cycling stability in aqueous electrolyte (Figure 30b). Pang et al. have developed $NaTi_2(PO_4)_3$–graphene nanocomposites as anode material for ASIBs.[72] The $NaTi_2(PO_4)_3$–graphene nanosheets (GNS) nanocomposite electrodes achieved discharge capacities of 86.7, 62.4, and 41.5 mA h g^{-1} at rates of 5, 10, and 20 C, respectively, and 90% of initial capacity was remained at 2 C after 100 cycles (Figure 30c,d).

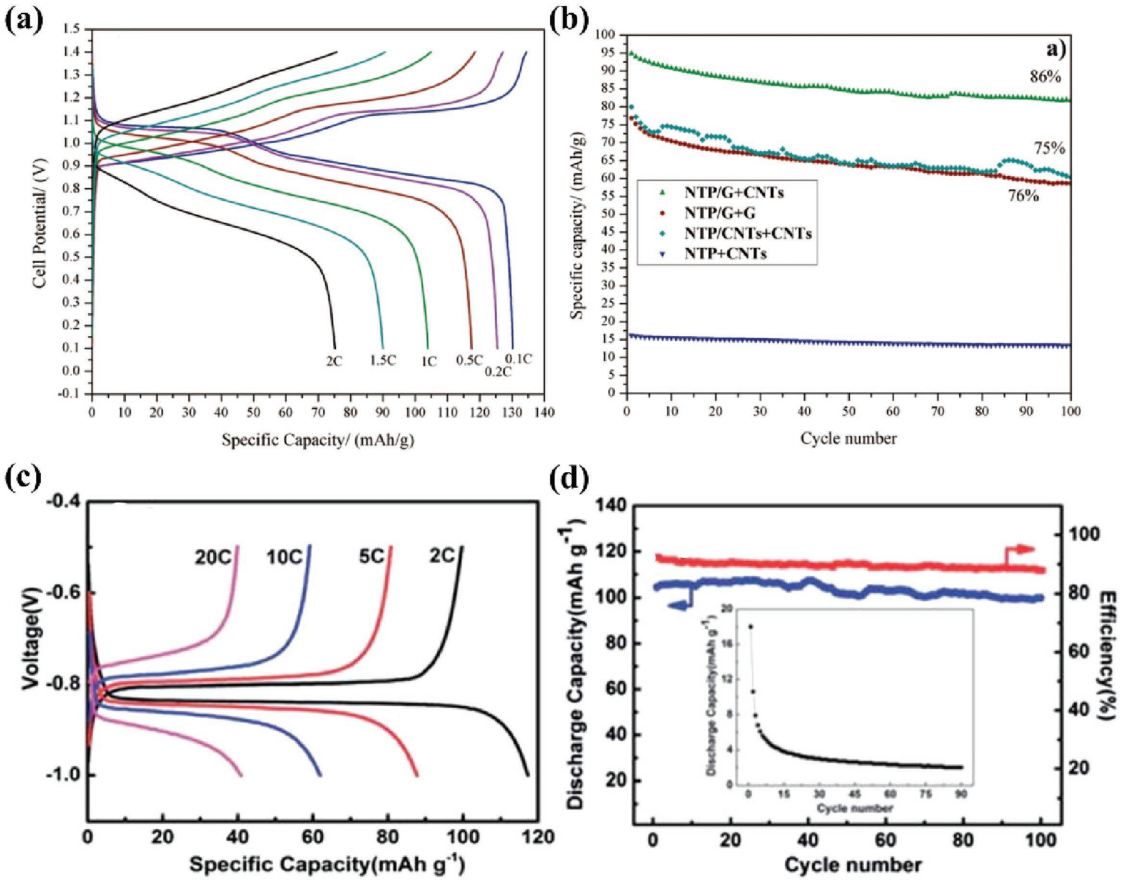

Figure 30. a) The typical voltage profile of the full aqueous Na-ion cell employing NTP/G + CNTs and $Na_{0.44}MnO_2$ as anode and cathode, respectively. b) Discharge capacity versus cycle number of different samples (NTP/CNTs+CNTs, NTP/G+CNTs, and NTP/G+G). Reproduced with permission.[71] Copyright 2014, ECS. c) Capacity–voltage profiles of $NaTi_2(PO_4)_3$–GNS at different current densities. d) Galvanostatic charge–discharge curves for $NaTi_2(PO_4)_3$–GNS at 2 C. The inset shows discharge capacity profile for pure $NaTi_2(PO_4)_3$ at 2 C. Reproduced with permission.[72] Copyright 2014, RSC.

In addition, Li et al. investigated the influence of varying graphene contents of $NaTi_2(PO_4)_3$–graphene composites on the electrochemical performance of ASIBs.[73] They have found that the 6.84% graphene-contained $NaTi_2(PO_4)_3$ sample displayed a high capacity of 129.3 mA h g^{-1} at 1 C, and a capacity of 55 mA h g^{-1} at a highest rate of 40 C, indicating its superior rate capability (**Figure 31**a). The composite also exhibited a high capacity of 63.5 mA h g^{-1} at 20 C, retaining 71% of the initial capacity after 2000 cycles (Figure 31b). To prevent unwanted side reactions. Mohamed et al. introduced polypyrrole as a coating for $NaTi_2(PO_4)_3$ through a high-energy ball-milling process.[74] Compared with the uncoated material, the coated $NaTi_2(PO_4)_3$ composites exhibited much better capacity retention, remaining 57% of the initial discharge capacity at the end of 50 cycles (Figure 31c,d).

In addition to all these, $NaTi_2(PO_4)_3$ with various morphologies, including wafer-like porous $NaTi_2(PO_4)_3$ decorated with hierarchical carbon, $NaTi_2(PO_4)_3$ thin-film electrodes, frogspawn-inspired hierarchical porous $NaTi_2(PO_4)_3$–C array, and $NaTi_2(PO_4)_3$ nanoparticles, have been reported as efficient anode materials for ASIBs.[75–78] Most recently, our group also designed a highly safe flexible ASIB based on a nanosized $NaTi_2(PO_4)_3$@C (NTPO@C) anode and NMO cathode in various Na^+-containing aqueous electrolytes. This novel fiber-shaped morphology equipped with aligned CNT/NMO and CNT/NTPO@C hybrid fibers as electrodes, in which the active materials (NMO or NTPO@C) were closely incorporated within the aligned CNT fibers by a wet twist process.[79] The galvanostatic charge–discharge curves of the flexible full cell tested in 1 M Na_2SO_4 electrolyte in the potential window of 0–1.6 V is shown in **Figure 32**a. A discharge specific capacity of 46 mA h g^{-1} was obtained at a current density of 0.1 A g^{-1}. At a high applied current density of 3 A g^{-1}, a reasonable capacity of 12 mA h g^{-1} was achieved, revealing its good rate capability. The cycle profile in Figure 32b indicates that 76% the initial capacity of the full cell was still maintained even after 100 cycles at a current density of 0.2 A g^{-1}. Attracted by the high flexibility of fiber-shaped ASIBs, it was found that the electrochemical performance of this full cell remained unchanged even after bending at 180° for 100 times (Figure 32c). Previous studies have demonstrated that $NaTi_2(PO_4)_3$ was quite stable in neutral pH electrolytes but unstable in alkaline electrolytes.[80] Recently, Mohamed and Whitacre systematically studied the inherent chemical stability of $NaTi_2(PO_4)_3$ in aqueous solutions at different pH and temperature.[81] **Figure 33**a shows the equilibrium solubility of $NaTi_2(PO_4)_3$ at various alkaline aqueous solutions. At 25 °C, the solubility of $NaTi_2(PO_4)_3$ was quite low at pH lower than

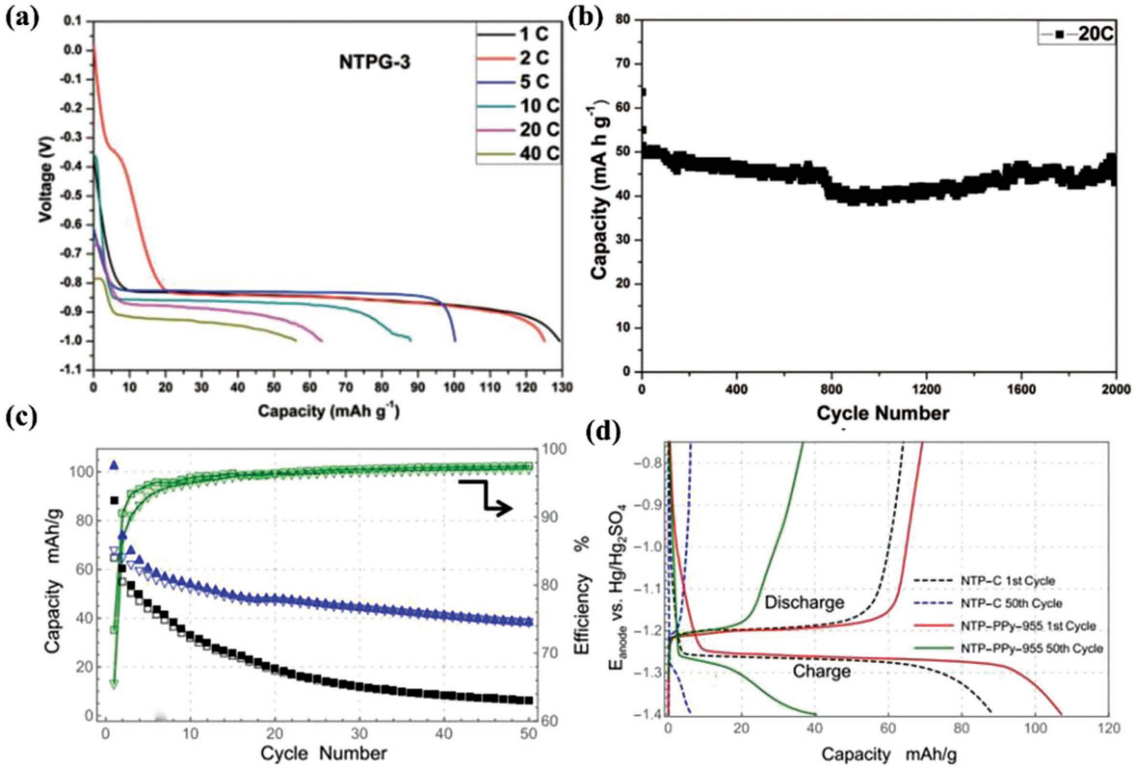

Figure 31. a) Discharge curves of the optimized $NaTi_2(PO_4)_3$/graphene composites in 1 M Na_2SO_4 aqueous electrolyte at various C rates. b) Discharge capacity versus cycle number at 20 C rate of $NaTi_2(PO_4)_3$/graphene composites. Reproduced with permission.[73] Copyright 2014. ECS. c) Charge–discharge curves for the 1st and 50th cycles of the $NaTi_2(PO_4)_3$-carbon and NTP-PPy-955. d) Cycling performance of NTP-C (uncoated) and NTP-PPy-955 (polypyrrole coated) and their corresponding efficiency. Reproduced with permission.[74] Copyright 2014, ECS.

11. When the pH reached 13.8, the concentration of dissolved titanium was lower than expected, owing to the precipitation of another phase. Interestingly, as observed in Figure 33b, the $NaTi_2(PO_4)_3$ prepared at 25 °C displayed a higher capacity than all samples prepared at 70 °C under galvanostatic cycling with potential limitation. These results obtained also indicated that the dissolution of $NaTi_2(PO_4)_3$ in alkaline solutions appeared to cause some amount of capacity fading, though the capacity loss was not as severe as has been reported in the literature.

3.2. Carbonyl-Based Organic Compounds

To fill the huge gap of need of efficient anode materials for ASIBs, several efforts have been focused on exploring other potential materials such as organic-based compounds. Although organic electrode materials have been reported for 30 years in the field of SIBs, 1,4,5,8-naphthalenetetracarboxylic dianhydride (NTCDA)-derived polyimide was first proposed by Qin et al. as anode material in ASIBs in 2014.[47,82–84] It has

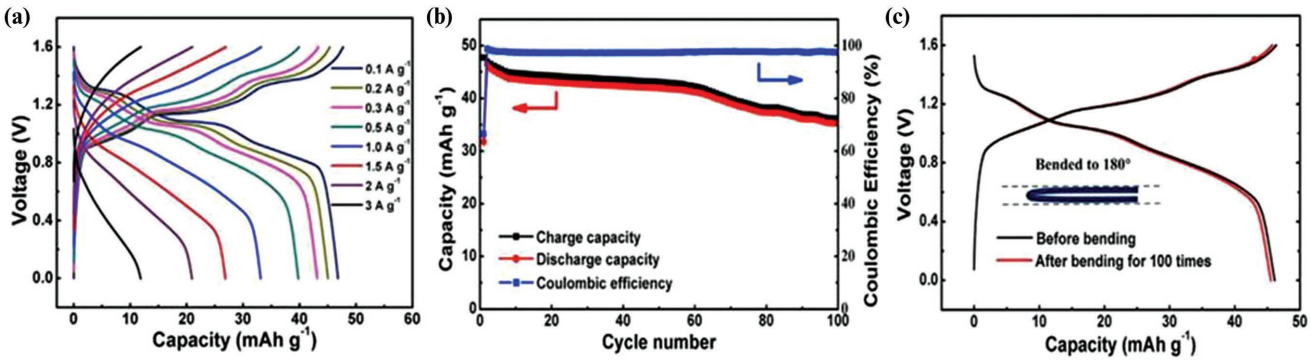

Figure 32. a) Galvanostatic charge/discharge curves of the fiber-shaped aqueous CNT/NMO//CNT/NTPO@C cells at different current densities. b) Capacity stability of the full cell aqueous SIBs at a current density of 0.2 A g^{-1}. c) Galvanostatic charge/discharge curves before and after bending of the flexible fiber-shaped ASIBs at a current density of 0.2 A g^{-1}. Reproduced with permission.[79] Copyright 2017, Elsevier.

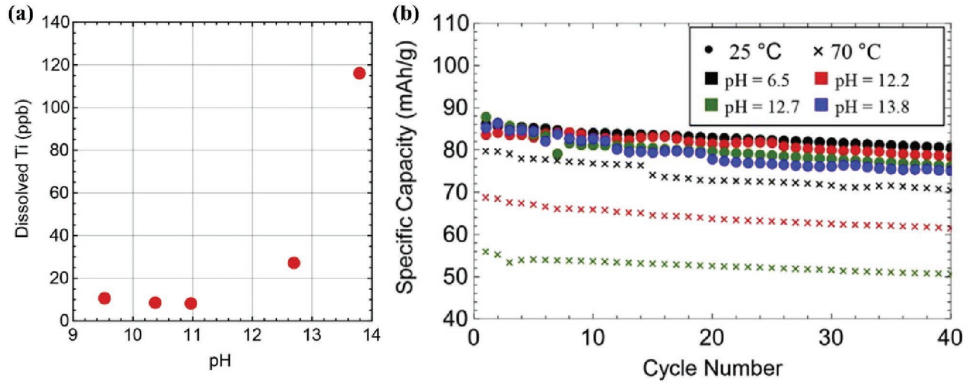

Figure 33. a) Total dissolved titanium from $NaTi_2(PO_4)_3$ in alkaline aqueous solutions. b) The cycle performance of the $NaTi_2(PO_4)_3$ in 1 M, neutral pH Na_2SO_4 solution at 25 and 70 °C after exposure in air. Reproduced with permission.[81] Copyright 2017, Elsevier.

been reported that the material mainly involved an enolization process when combining with Na^+-ion insertion/extraction in 5 M $NaNO_3$ solution at a potential of ≈0.5 V versus SCE, accompanied with the charge redistribution within the conjugated aromatic molecule, as illustrated in **Figure 34**a. The electrode performance of polyimide was further investigated in some later studies. For example, Deng et al. have synthesized a redox active and water-insoluble polyimide, poly-(naphthalene-4-formyl ethylenediamine) (PNFE), exhibiting two reduction peaks at –0.55 and –0.9 V (Figure 34b) during the Na^+ ion insertion process due to the reversible two-electron redox reaction in the polymer chains. A high capacity up to 140 mA h g^{-1} was demonstrated at a current density of 0.1 A g^{-1} (Figure 34c).[85] The reversible capacity of the PNFE electrode decreases from 134 to 112 mA h g^{-1} when the current rate increased from 1 to 12 C and maintains a reversible capacity of ≈95 mA h g^{-1} at 18 C (Figure 34d). Moreover, long-term cycling stability of PNFE was evaluated at a constant current of 10 C between –1.0 and 0 V, and remarkable stability with almost no discernible capacity decay after 1000 cycles was demonstrated (Figure 34e).

Recently, Gu et al. have prepared a polyimide–MWCNT composite (PNP@CNT) synthesized from NTCDA anode and $Na_{0.44}MnO_2$ cathode, to serve as ASIB materials.[86] The PNP@CNT/NMO full cell delivered a reversible capacity of 92 mA h g^{-1} (normalized to anode capacity), with a discharge voltage of 0.8 V, as shown in **Figure 35**a. This full cell can be well cycled at a high rate of 5 C for over 200 cycles, delivering an energy density of 25 Wh kg^{-1} (Figure 35b). Quinones, especially 1,2-benzoquinone or 1,4-benzoquinone, have brought immense opportunities in organic-based energy storage systems such as nonaqueous metal-ion batteries, as well as aqueous flow batteries due to their structurally stable ion-coordination charge storage mechanism and chemical inertness.[87,88] In 2017, Liang et al. have reported several typical quinones (pyrene-4,5,9,10-tetraone, polymeirzed pyrene-4,5,9,10-tetraone (PPTO), poly (anthraquinonyl sulfide)) as stable anode materials. Their operational pH values (–1 to 15) allowed them to be universal charge carrier species (H^+, Li^+, Na^+, K^+, and Mg^{2+}) for aqueous battery technology.[89] As shown in Figure 35c, a prototype quinone-based ASIB with PPTO (anode)–$Na_3V_2(PO_4)_3$ (cathode) configuration showed high anode specific capacity (201 mA h g^{-1}) and 79% capacity retention up to 80 cycles in a neutral $NaNO_3$ electrolyte (Figure 35d).

3.3. Vanadium-Based Materials

Since VO_2 was first specified as the anode of aqueous lithium-ion battery by Dahn and co-workers in 1994, other vanadium-based materials have also been demonstrated as anode material for ASIBs.[11] V-based materials are of particular interest owing to the various oxidation states accessible, achieving multi-electron redox reactions. As reported by Wu co-workers, the $V_2O_5 \cdot 0.6H_2O$ nanoribbons anode material enabled the insertion of three alkali metal cations (Li^+, Na^+, and K^+), and the highest capacity was observed in K_2SO_4 solution.[90]

In addition, Deng et al. have demonstrated nanostructured layered Na–vanadium oxide ($Na_2V_6O_{16} \cdot nH_2O$), whereby the hydrated Na ions are located at the interstices between V_3O_8 layers, as a novel anode material for ASIBs.[91] However, the $Na_2V_6O_{16} \cdot nH_2O$ delivered initial discharge and charge capacities of 123 and 42 mA h g^{-1} respectively, indicating a very low initial Coulombic efficiency of 45% (**Figure 36**a). Furthermore, the discharge (Na intercalation) capacity diminished quickly in the first few cycles and then stabilized upon further cycling (Figure 36b). Using ex situ X-ray diffraction measurement, it was justified that this fast capacity fading could be attributed to the irreversible phase transition which mainly occurs in the first discharge process. Recently, Ke et al. investigated a series of potential aqueous Na anode materials such as low carbon aggregated $NaV_3(PO_4)_3$ powder, $NaV_3(PO_4)_3$/C random arranged nanofiber, and well-aligned $NaV_3(PO_4)_3$/C nanofiber.[92] Higher capacities at different current densities were obtained for the aligned nanofiber $NaV_3(PO_4)_3$/C compared with another two materials (random arranged nanofiber and the low-carbon aggregated powders), as displayed in Figure 36d. It could also deliver reversible capacities of ≈148 and ≈60 mA h g^{-1} at the 0.5 and 25 C rates, respectively (Figure 36c). Moreover, the well-aligned nanofiber achieved higher capacity retentions of 95.9% and 94.2% at low (1 C)

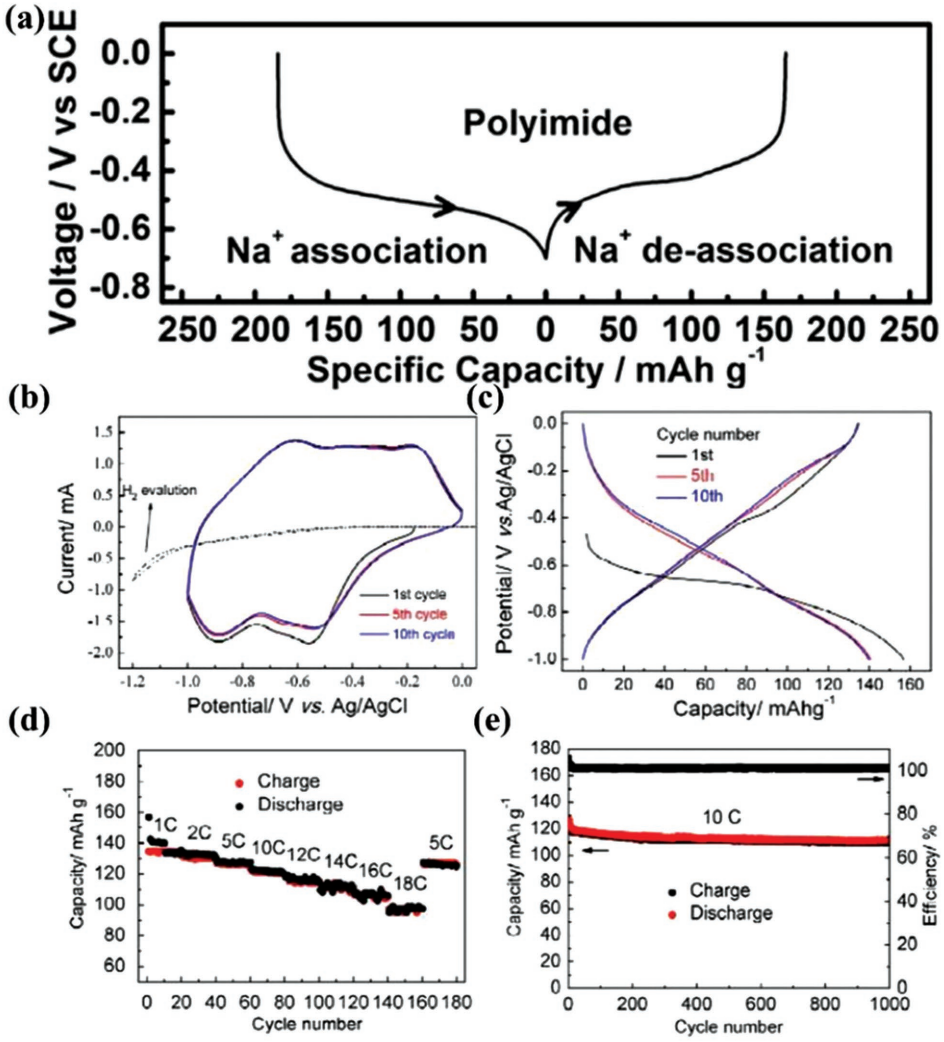

Figure 34. a) Polyimide electrode in 5 M $NaNO_3$ aqueous electrolyte at a current density of 50 mA g^{-1}. Reproduced with permission.[47] Copyright 2014, Elsevier. b) CV curves the PNFE electrode measured in aqueous electrolyte at a scan rate of 10 mV s^{-1}. c) Charge/discharge profiles in the first ten cycles at a current density of 0.1 A g^{-1}. d) Reversible capacities cycled at various rates from 1 to 18 C for the PNFE electrode. e) The corresponding long-term cycling stability at a constant current of 10 C between −1.0 to 0 V. Reproduced with permission.[85] Copyright 2015, RSC.

and high (10 C) rates, respectively. These results are much higher than the random aligned reference (89.1% at 1 C and 82.4% at 10 C) and the low-carbon aggregated samples reference (80.9% at 1 C and 71.6% at 10 C) (Figure 36e). As an important class of NASICON electrode material, the above-mentioned $Na_2VTi(PO_4)_3$ material could be used in symmetric AISB systems as both the cathode and anode because of its multiple redox couples (V^{3+}/V^{4+}, Ti^{4+}/Ti^{3+}). The Na^+ insertion process of $Na_2VTi(PO_4)_3$ is presented as follows: $Na_2V^{3+}Ti^{4+}(PO_4)_3 + xNa^+ + e^- \leftrightarrow Na_{2+x}V^{3+}Ti^{4+}(PO_4)_3$.

3.4. Other Compounds

As discussed in the above section, PBAs and their derivatives have always used as the cathode materials for ASIBs. Even more interesting is the previous reported cell by Cui and co-workers, in which manganese hexacyanomanganate, an open-framework structure of Prussian blue analogs, was also investigated as anode material for ASIBs for the first time.[93] The newly developed Mn-based Prussian blue analog (Mn^{II}–NC–$Mn^{III/II}$) anode was then coupled with a copper hexacyanoferrate (Cu^{II}–NC–$Fe^{III/II}$) cathode to assemble an asymmetric cell, as illustrated in **Figure 37**a. Figure 37b shows that the Mn^{II}–NC–$Mn^{III/II}$ anode exhibited similar capacities at different C rates (1, 5, and 10 C) that reach up to ≈50 mA h g^{-1}, indicating a high rate capability. Furthermore, extended cycling of the full battery that contains an Mn^{II}–NC–$Mn^{III/II}$ anode and a Cu^{II}–NC–$Fe^{III/II}$ cathode displayed 99.8% Coulombic efficiency and no measurable capacity loss after 1000 cycles at a 10 C rate (Figure 37c).

A new type of MoO_3 nanobelt-coated polypyrrole has also been reported as anode material for ASIBs by Wu and co-workers.[94] CV curves in **Figure 38**a showed that the two sets of redox potentials situated at −0.25/−0.08 V and −0.49/−0.34 V

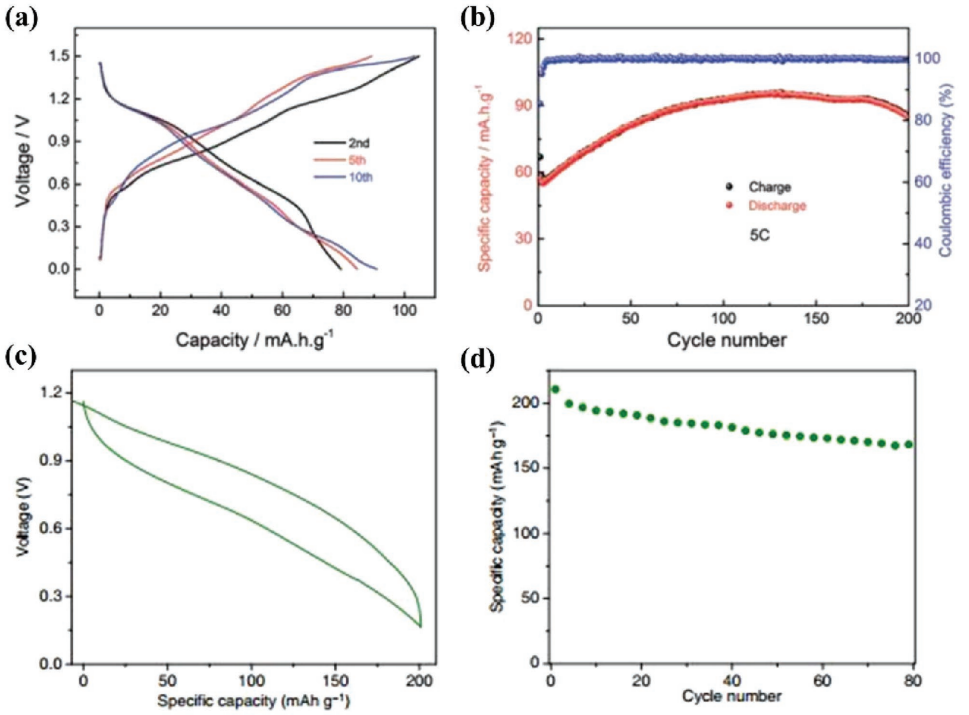

Figure 35. Electrochemical performances of the PNP@CNTs/NMO full cell. a) The charge–discharge profiles in first ten cycles at a current density of 1 C. b) Long-term cycling stability at a constant current of 5 C. Reproduced with permission.[86] Copyright 2016, RSC. c) Galvanostatic charge–discharge profile and d) cycling performance of a PPTO–$Na_3V_2(PO_4)_3$ aqueous Na full cell measured in 5 M $NaNO_3$ (pH 7) at 1 C. Reproduced with permission.[89] Copyright 2017, Macmillan Publishers Ltd.; Nature Materials.

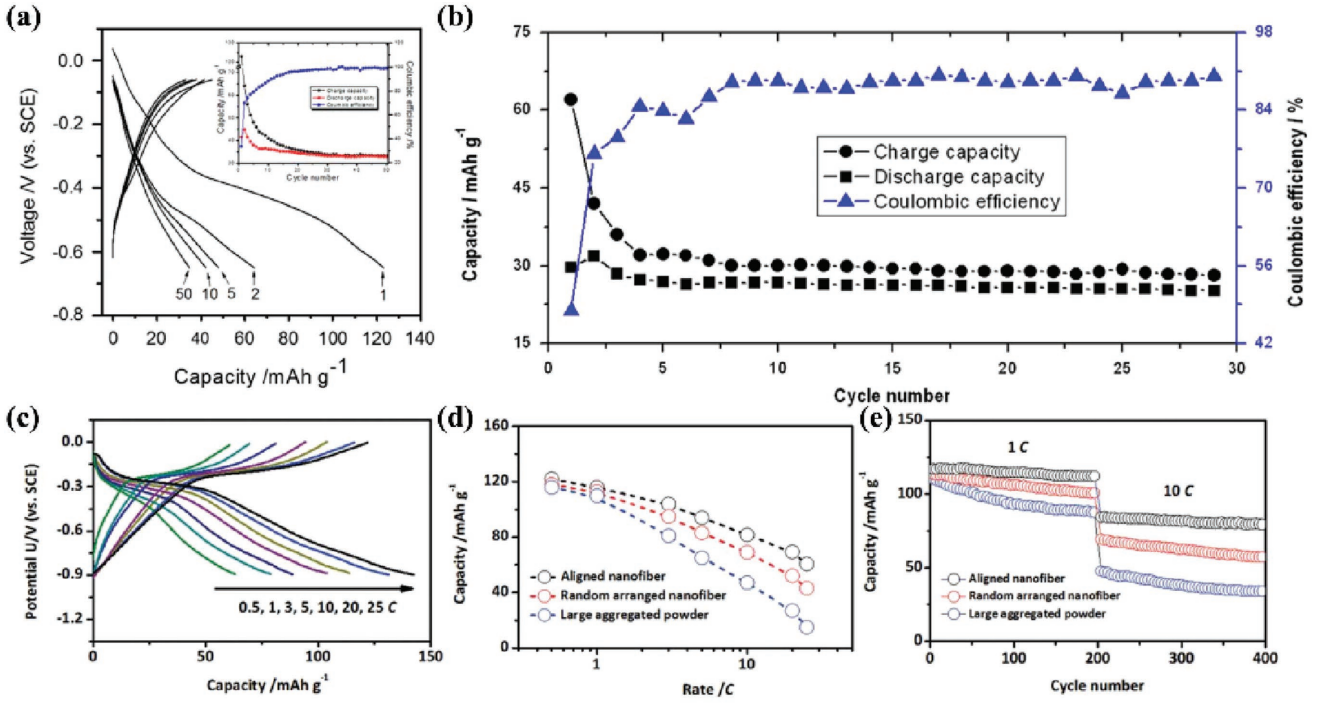

Figure 36. a) Galvanostatic discharge–charge curves at different current density of the 1D nanostructured $Na_2V_6O_{16}{\cdot}nH_2O$. b) The Coulombic efficiency as a function of cycle number of the aqueous full cell based on the $Na_{0.44}MnO_2$ cathode and the $Na_2V_6O_{16}{\cdot}nH_2O$ anode. Reproduced with permission.[91] Copyright 2014, Elsevier. c) Galvanostatic charge/discharge curves of the aligned $NaV_3(PO_4)_3$ nanofiber at different rates. d) Comparison of the rate capability of the aligned nanofiber, random arranged nanofiber, and large aggregated powder reference samples. e) Cycling properties of different $NaV_3(PO_4)_3$ samples at high (10 C) and low (1 C) rates. Reproduced with permission.[92] Copyright 2017, RSC.

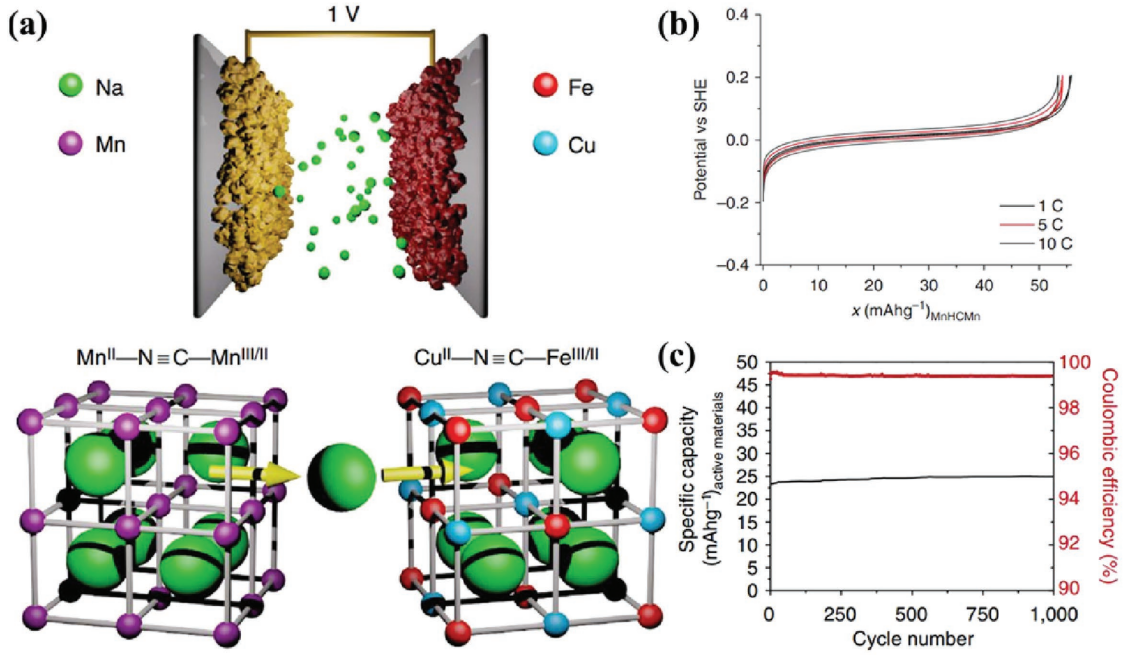

Figure 37. a) Schematic representation of symmetric open-framework full cell, based on the integration of copper hexacyanoferrate (Cu^{II}–NC–$Fe^{III/II}$) cathode and the newly developed manganese hexacyanomanganate (Mn^{II}–NC–$Mn^{III/II}$) anode. b) Charge/discharge profiles of Mn^{II}–NC–$Mn^{III/II}$ at 1, 5, and 10 C rates. c) Cycle performance of the full cell at a 10 C rate in 10 M $NaClO_4$ electrolyte. Reproduced with permission.[93] Copyright 2014, Macmillan Publishers Ltd.; Nature Communication.

(vs SCE) for polypyrrole (PPy)@MoO_3 are observed when tested in 0.5 M Na_2SO_4 solution, corresponding to the reversible intercalation/de-intercalation of Na^+ ions into/from the MoO_3 host. The cycling behavior of full cell consisting of PPy@MoO_3 anode and $Na_{0.35}MnO_2$ cathode is displayed in Figure 38b. The full cell displayed 21% capacity loss in the first few cycles of the total 1000 cycles. Most recently, another NASICON-structured porous $Na_3MgTi(PO_4)_3$ has been investigated as the anode material for ASIBs.[95] As shown in **Figure 39**a, this porous $Na_3MgTi(PO_4)_3$ shows an initial discharge capacity of 61 mA h g^{-1} at 0.2 C, which accounts for 97% of theoretical capacity (62.8 mA h g^{-1}). Due to the porous nature of the material and the fast ionic diffusivity, good rate capability was demonstrated (Figure 39b), where the capacities at 0.5, 1, 2, and 4 C were 93%, 85%, 75%, and 61% of the capacity at 0.2 C, respectively. Similar to the Ti^{4+}/Ti^{3+} redox couple in $NaTi_2(PO_4)_3$, the $Na_3MgTi(PO_4)_3$ showed a capacity retention of 94.2% after 100 cycles in 6 M $NaClO_4$ solution, superior to the $NaTi_2(PO_4)_3$ prepared with the same method (Figure 39c). Commonly, the $Na_{0.44}MnO_2$ was extensively utilized as the cathode material in ASIBs due to its excellent stability in aqueous solution. In view of the anode materials, however, Wang et al. show that the Ti-substituted $Na_{0.44}MnO_2$ ($Na_{0.44}[Mn_{1-x}Ti_x]O_2$) with tunnel structure can be used as a negative electrode material for

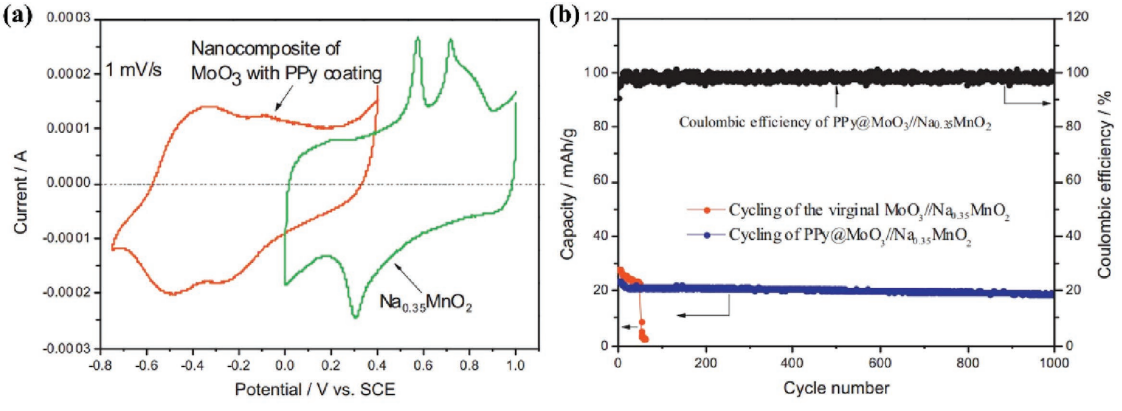

Figure 38. a) CV curves of the nanocomposite of MoO_3 coated with PPy and the nanowire $Na_{0.35}MnO_2$ at a scan rate of 1 mV s^{-1} in 0.5 M Na_2SO_4 solution. b) The cycling behavior of full cell based on PPy@MoO_3 anode and $Na_{0.35}MnO_2$ cathode at 0.55 A g^{-1}. Reproduced with permission.[94] Copyright 2014, Elsevier.

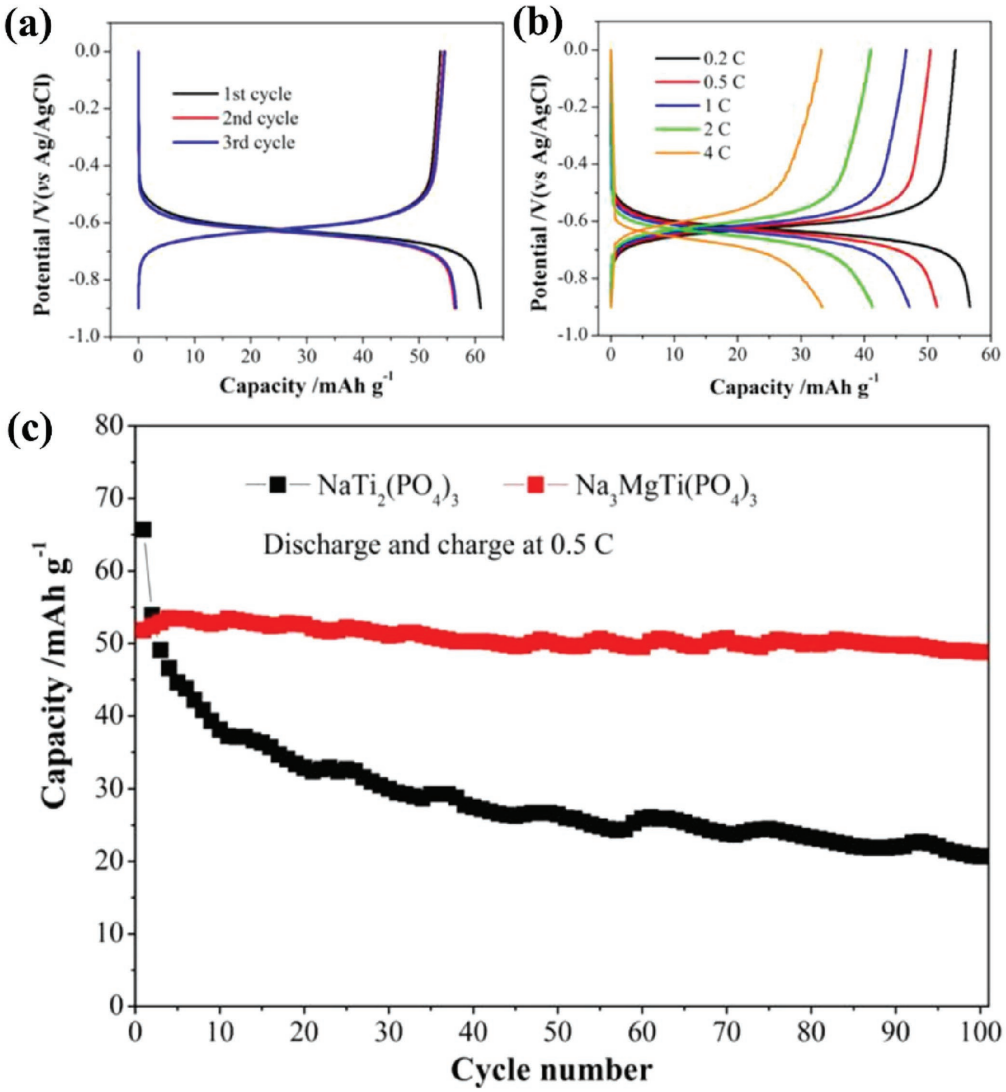

Figure 39. Charge/discharge profiles of $Na_3MgTi(PO_4)_3$ material obtained a) at a current rate of 0.2 C and b) at various current rates in 6 M $NaClO_4$ solution. c) Cycling performance of the $Na_3MgTi(PO_4)_3$ and traditional $NaTi_2(PO_4)_3$ at 0.5 C. Reproduced with permission.[95] Copyright 2017, Wiley.

ASIBs.[96] In order to smooth the charge/discharge and lower the storage voltage, they tuned the charge ordering property and reaction pathway by Ti substitution, which was clearly demonstrated on an atomic scale. Among these Ti-substituted $Na_{0.44}[Mn_{1-x}\ Ti_x]O_2$ (x = 0.11, 0.22, 0.33, 0.44, and 0.56) materials, they found that a stable capacity of 37 mA h g^{-1} can be reached for the $Na_{0.44}[Mn_{0.44}Ti_{0.56}]O_2$ at 2 C rate in aqueous electrolyte (**Figure 40**a). As further manifested in Figure 40b, the $Na_{0.44}[Mn_{0.44}Ti_{0.56}]O_2$ anode material also suggests great cycling performance with no evident capacity fading after 400 cycles, even without taking special caution to remove the oxygen in aqueous electrolyte.

So far we have made successful discussions on the electrochemical behaviors of various cathode and anode materials for the ASIBs. To systematically compare the electrochemical properties of the full cell configurations of electrode materials for ASIBs, we have categorized them on the basis of on their major parameters, including average operating voltages, specific capacities, and cycling performance, as shown in **Table 1**.

4. Electrolytes

Electrolytes, as ion transport intermediate between electrodes, provide an ion pathway to support the current.[98,99] The liquid electrolytes are traditionally prepared by dissolving salt into proper solvents. Water is an attractive alternative compared to the nonaqueous solvents, because it is not only intrinsically safe, but also an excellent solvent with both high acceptor and donor numbers. Therefore, aqueous electrolytes have usually an order magnitude higher ionic conductivity than nonaqueous electrolytes in a given conxcentration, making it possible to achieve high power storage systems.[4] Coupled with the abundance of Na element, ASIBs are promising for large-scale electric energy storage applications.

4.1. Diluted Electrolytes

Due to the coexistence of Lewis basicity of its oxygen site and Lewis acidity of its hydrogen site, water could solvate most salts

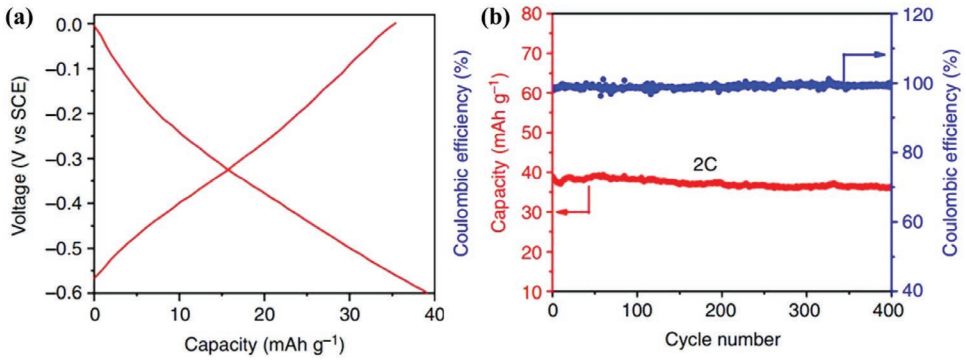

Figure 40. a) The first discharge/charge curves in the voltage range of –0.6 and 0 V versus SCE for $Na_{0.44}[Mn_{0.44}Ti_{0.56}]O_2$ electrode at a current rate of 2 C, and b) the corresponding long-term cycling performance at 2 C. Reproduced with permission.[96] Copyright 2015, Macmillan Publishers Ltd.; Nature Communication.

to form the solvation structure. In the Na^+ dilute solutions, the primary and secondary solvation shells typically contain an Na-ion coordinated with six water molecules, due to largely free water molecules available.[100] Traditionally, the dilute Na-ion solutions are employed as the electrolytes for ASIBs due to their high ionic conductivity and low cost.

1 M Na_2SO_4 is the most reported electrolyte for ASIBs and compatible with various electrode materials in neutral pH, including the $Na_{0.44}MnO_2$,[21,22] $Na_3V_2(PO_4)_3$,[41] $Na_3MnTi(PO_4)_3$,[44] $NaTi_2(PO_4)_3$,[101–102] and so on. As in the water Pourbaix diagram, the stability window will shift to a lower potential with increasing pH value, thus enabling more anode electrode materials to embrace into stable electrolyte windows. For example, $Na_{0.44}[Mn_{0.44}Ti_{0.56}]O_2$ was tested as a stable cathode material in the Na_2SO_4 with a pH of 13.5. Besides Na_2SO_4, 1 M $NaNO_3$[103] and 1 M CH_3COONa[73,104] have also been employed in previous reports. Recently, 1 M NaCl solution was shown as an effective electrolyte choice to build an ASIB with good biocompatibility.[79]

4.2. Concentrated Electrolytes

Despite the safety and low cost, the narrow thermodynamic stability window (1.23 V) of water precludes the application of high-voltage electrode couples, thus limiting the energy density of the ASIBs. For the same reason, the water consumption (decomposition) always happens that can lead to the failure of sealed aqueous battery system. Besides the electrolyte decomposition, other side reactions are also involved, including the reaction between electrode and water or O_2, proton cointercalation, and the dissolution of electrode materials.[70]

To some extent, all the above-mentioned shortcomings could be virtually eliminated by employing concentrated electrolytes,

Table 1. Summary of the electrochemical properties of typical full cell configurations for ASIBs.

Cathode	Anode	Electrolyte	Current rate	Voltage [V]	Capacity [mA h g^{-1}]	Retention [%/cycles]	Ref.
$Na_{0.44}MnO_2$	$NaTi_2(PO_4)_3$	1 M Na_2SO_4	5 C	1.1	95	86% (100)	[97]
$Na_{0.66}[Mn_{0.66}Ti_{0.34}]O_2$	$NaTi_2(PO_4)_3$	1 M Na_2SO_4	2 C	1.2	76	≈87% (300)	[24]
$NaMnO_2$	$NaTi_2(PO_4)_3$	2 M CH_3COONa	5 C	≈1.0	27	75% (500)	[28]
$K_{0.27}MnO_2$	$NaTi_2(PO_4)_3$	1 M Na_2SO_4	0.2 A g^{-1}	≈1.2	68.5	No decay (100)	[30]
$Na_3V_2(PO_4)_3$	$NaTi_2(PO_4)_3$	1 M Na_2SO_4	10 A g^{-1}	1.2	58	50% (50)	[42]
$Na_2VTi(PO_4)_3$	$Na_2VTi(PO_4)_3$	1 M Na_2SO_4	10 C	≈1.2	40.6	≈70% (1000)	[45]
$Na_3MnTi(PO_4)_3$	$Na_3MnTi(PO_4)_3$	1 M Na_2SO_4	1 C	1.4	56.5	≈98% (100)	[44]
$Na_3V_2O_2(PO_4)$F-MWCNT	$NaTi_2(PO_4)_3$-MWCNT	10 M $NaClO_4$ + 2% VC	1 C	1.5	54.3	≈81% (100)	[46]
$NaVPO_4F$	Polyimide	5 M $NaNO_3$	0.05 A g^{-1}	0.8	54	≈68% (20)	[47]
$Na_2CuFe(CN)_6$	$NaTi_2(PO_4)_3$	1 M Na_2SO_4	10 C	1.4	86	≈88% (1000)	[60]
$Na_2NiFe(CN)_6$	$NaTi_2(PO_4)_3$	1 M Na_2SO_4	5 C	1.3	79	≈88% (250)	[59]
$Na_{0.44}MnO_2$	Polyimide-MWCNT	1 M Na_2SO_4	5 C	0.8	60	No decay (200)	[86]
$Na_{0.44}MnO_2$	$Na_2V_6O_{16}\cdot nH_2O$	1 M Na_2SO_4	0.04 A g^{-1}	0.8	30	≈67% (250)	[91]
$Na_{0.44}MnO_2$	$NaV_3(PO_4)_3$@C	1 M Na_2SO_4	5 C	0.7	100	≈83% (500)	[92]
$Na_{0.35}MnO_2$	PPy@MoO_3	0.5 M Na_2SO_4	0.55 A g^{-1}	0.8	25	≈79% (1000)	[94]
Cu^{II}-NC-$Fe^{III/II}$	Mn^{II}-NC-$Mn^{III/II}$	10 M $NaClO_4$	10 C	1.0	22	No capacity loss (1000)	[93]

Table 2. The solubility for several common-used Na salts at the temperature of 20 °C. (The molality is calculated based on the solubility.)

Electrolyte	Solubility [g/100 g H_2O]	Molality [mol kg^{-1}]
CH_3COONa	46.4	5.7
NaCl	35.9	6.1
$NaNO_3$	87.6	10.3
Na_2SO_4	19.5	1.4
$NaClO_4$	201	16.5

in which the water activity is strongly suppressed. Encouraging results have been demonstrated that highly concentrated Li-ion electrolytes expand the electrolyte stability window and stabilize the electrode performance.[105,106] Many researchers have paid attention to the relationship between the electrolyte concentration and the electrochemical performance of ASIBs.[78,107,108] For concentrated Na-ion aqueous electrolytes, the mild solubility of Na_2SO_4 restricts the formation of concentrated electrolyte (**Table 2**). On the other hand, highly concentrated 5 M $NaNO_3$ has been reported, while the corrosive side reactions were also observed.[47] Na-bis(fluorosulfonyl)imide (NaFSI) was reported with ultrahigh solubility in water up to 37 M and could support a wide stability window,[109] whereas the stability of FSI^- anion in the water remains a concern.

Concentrated $NaClO_4$ solution is a very distinctive electrolyte for ASIBs and has received immense interests recently.[110–113] As shown in Table 2, $NaClO_4$ has a very high solubility. The saturated $NaClO_4$ electrolyte was reported with a remarkable wide electrochemical window of around 3.2 V. Despite the fact that exactness of the window remains controversial, it can undoubtedly play a vital role to overcome vulnerability caused by the narrow window for ASIBs and enable more electrode couples.[107]

Recently, the concept of "water-in-salt" (WiS) approach has been used in Na-ion aqueous electrolyte using 9.26 m Na trifluoromethane sulfonate ($NaCF_3SO_3$).[114] Although the concentration of Na-based WiS is incomparable to the lithium-based WiS electrolyte due to the limitation of Na-salt solubility, interestingly, the stable electrolyte window still successfully expands into 2.5 V. This enables us to suppress the hydrogen evolution on anode with the formation of an Na^+-conducting SEI and reduce the overall electrochemical activity of water on cathode. An $Na_{0.66}[Mn_{0.66}Ti_{0.34}]O_2/NaTi_2(PO_4)_3$ full cell using Na-WiS exhibited superior performance, as exemplified by extraordinarily high Coulombic efficiency (>99.2%) at a low rate (0.2 C) for >350 cycles, and excellent cycling stability at a high rate (1 C) for >1200 cycles.

5. Challenges and Future Outlook

Although ASIBs have been developed as promising alternatives for conventional organic Na-ion batteries by virtue of the above-discussed advantages, there are many scientific and technical challenges that hinder in making large-scale application, mainly including H_2/O_2 evolution reactions from aqueous electrolyte, the electrode reaction with the water or O_2, the dissolution of electrode in water and proton cointercalation. Here, we conclude all of the challenges that limit the choice of electrode materials in ASIBs.

5.1. H_2/O_2 Evolution Reactions from Aqueous Electrolyte

Water splitting from aqueous electrolyte, $2H_2O \rightarrow 2H_2 + O_2$, has two related half-reactions: HER OER. Thermodynamically, the electrochemical stability window of aqueous electrolyte is limited to be 1.23 V without the effect of overpotential. Taking into account the H_2/O_2 evolution reaction, the Na^+ extraction/insertion potential of the electrode materials (both anode and cathode) should be occurred within the water stability window. The electrolysis overpotential of water generally depends on the relative activity of water-splitting catalysts, that is to say, the catalytic activity of electrode must be as low as possible. In order to increase energy density by enlarging the low operation window of water (1.23 V), kinetics are key points in minimizing electrolyte breakdown in lead–acid batteries, hence enabling an operating voltage in water of up to ≈2.2 V. In this context, a recent paper by Suo et al. reported extending the operation window of aqueous electrolytes to 3 V via a highly concentrated "water-in-salt" electrolyte,[105] providing different strategies to suppress H_2/O_2 evolution reaction and potentially resulting in a significant enlightenment in ASIBs.

The stable SEI between the electrolyte and electrode could suppress the parasitic side reaction and significantly enhance the cyclability of the battery. In nonaqueous battery systems, the formation of SEI was typically supported by the decomposition of the organic solvents and salts. Unfortunately, the decomposition of water cannot form a dense interphase on the surface.[115] Therefore, introduction of a third component (additive) to form the interphase may be an effective approach, which has been very popular in nonaqueous Li-ion batteries, and needs to be paid more attention. Besides that, the compatibility between the electrode materials and Na salts and the pH values of an aqueous electrolyte needs more detailed research.[116] Last but not least, the corrosion prevention and the choice of current collectors in the specific electrolytes should not be overlooked.[117]

5.2. The Electrode Reaction with Water or O_2

It is well known that the aqueous sodium-ion battery customarily occurs in air, thereby, the presence of H_2O and dissolved O_2 may oxidize some full intercalated anode materials. Similar to the condition in ALIBs, regardless of the pH of the electrolyte, none of the previous materials could be utilized as anode electrode for ASIBs in the presence of O_2. That is to say, the discharge state of anode materials would, theoretically, be chemically oxidized by the O_2 and H_2O rather that undergoing the electrochemical reaction, thereby leading to the unsatisfactory Coulombic efficiency and cycle stability.

As a typical example, the $NaTi_2(PO_4)_3$ material could not be used as aqueous anodes to keep superior long stability in an alkaline electrolyte, owing to the instability of Ti^{3+}. The cumulative effect of adjustment of the cutoff voltage at a certain pH, elimination of residual O_2 in the electrolyte, and carbon coating on the electrode is crucial for stable operation of aqueous batteries.

5.3. The Dissolution of Electrode in Water

Another essential aspect of poor cycling ability of ASIBs is the fact that some materials easily dissolve in water. Some vanadium-based compounds, especially the V^{5+} species, can hardly exist in the aqueous electrolyte. Related to this, some researchers have found that full coating technology and stabilization of the electrode surface using VC additives to form a stable SEI layer may prevent the dissolution of electrode.[46]

Concerns regarding the "green" quality of batteries are more aware than ever and have been addressed in a variety of ways over the years. It is no doubt that the ASIBs have emerged as the highly safe and environmentally friendly devices for ESSs. Although such systems have shown promising advantages, the relatively lower energy density due to the limited operating voltage of H_2O (≈1.2 V) compared to that of organic electrolyte systems is still the main challenge. The "rocking-chair" approach in ASIBs, identical to organic lithium-ion batteries, enables Na ion to intercalate reversibly into a sodium-accepting anode and deintercalate from sodium-source cathode without destroying the structure of the electrode materials. Various electrode materials, especially Na_xMnO_2 cathode and $NaTi_2(PO_4)_3$ anode, have also been widely studied as candidates for ASIBs. However, we are still far from the goal to develop a practical aqueous-based battery with both high specific capacity and long life. By optimizing the electrode design, adjusting the pH of the electrolyte, removing the dissolved oxygen, and employing advanced battery-assembly technologies, there are still huge opportunities to make the large-scale practical application of ASIBs possible.

5.4. Proton Cointercalation in Parallel with Sodium Intercalation

Similar to ALIBs, although some cathode material could be steadily existed in water, protons may be cointercalation into the electrode materials competed with sodium intercalation in ASIBs. The proton intercalation is related to the crystal structure and the pH of the electrolyte. One common strategy is modulating the potential for proton intercalation through adjusting the pH of the electrolyte. It can be found that most cathode materials occur stable sodium deinsertion/intercalation in neutral aqueous electrolytes, which is the potential alternative to explore minimal proton deinsertion/intercalation in ASIBs.

5.5. The Corrosion of Current Collectors

In aqueous solution, current collectors are usually consisted of nickel mesh, titanium mesh, aluminum, or stainless steel. As previously reported, the electrode/electrolyte interface is essential for optimizing the working parameters of electrochemical reaction, including hydrogen evolution and oxygen evolution. It should be pointed out that the current collectors may suffer some corrosion during the cycling in aqueous electrolyte. The corrosion processes can take place on positive and negative electrodes. Moreover, the choice of current collectors depends of the pH of the aqueous electrolyte. Usually, titanium mesh, a very stable material and has the large overpotential of oxygen evolution, can be used for both cathode and anode. The nickel mesh cannot be used in acidic media, since the Ni can react with the high concentration of H^+, and it cannot also be considered as the cathode in aqueous solution due to the low oxidation potential of Ni and Ni^{2+}. Recently, Wojciechowski et al. found that stainless steel working in 6 and 1 M KOH has the lowest corrosion potential, and the corrosion potential increases with decreasing pH value. This is caused by the high concentration of OH ions which behave as catalysts for the dissolution of steel components.[118] Most recently, Wang et al. found that aluminum foil armored by conformal graphene coating exhibited signifcant reinforced anodic corrosion resistance in both $LiPF_6$ and lithium bis(trifluoromethanesulfonyl) imide-based electrolytes.[119] The multilayered graphene films were grown on aluminum foil via plasma-enhanced chemical vapor deposition method, which served as extraordinary conductive shield that could efficiently thwart the attracts of the anions or the other coordinating species to Al^{3+}. Their result might open up new horizons for the corrosion of current collectors.

5.6. The Influence of Binders

Developing high-performance battery systems requires the optimization of the binder system, which is also needed to be noticeable in the ASIBs. Conventional binder systems consisting of nonconductive polymers and carbon additives provide functions of mechanical adhesion and conductive connection separately. In organic battery systems, PVDF is the most commonly used binder due to its binding capability, good electrochemical stability, and the capability of transport ion to the active materials' surface.[120] Recently, researchers have tried to consider polymers containing carboxylic materials such as carboxymethyl cellulose, poly-acrylic acid, and alginate as binders because they can promote the formation of a stable SEI layer and accommodate the volume change of active particles.[121] In aqueous system, polytetrafluoroethylene (PTFE) is an environmentally friendly polymer binder, which has always been used in aqueous battery field, or air cathode as a catalyst binder. However, the PTFE has big impedance and poor wettability with aqueous electrolyte. Yu et al. developed a conductive, healing hybrid gel by incorporating a supramolecule into conductive PPy gel matrix, which could heal cracks at room temperature without external stimuli.[122] Therefore, there should be adaptable work focused on the better binders which can improve the conductive of binders by introducing some conductive polymer materials.

Acknowledgements

The authors acknowledge funding support from the National Key Research and Development Program of China (Grant No. 2016YFB0901500) and the Natural Science Foundation of China (Grant No. 21333002).

Conflict of Interest

The authors declare no conflict of interest.

Keywords

aqueous sodium-ion batteries, challenges, development, electrochemical performance, power source

Received: October 29, 2017
Revised: January 16, 2018
Published online:

[1] C. P. Grey, J. M. Tarascon, *Nat. Mater.* **2016**, *16*, 45.
[2] B. Dunn, H. Kamath, J. M. Tarascon, *Science* **2011**, *334*, 928.
[3] H. Kim, J. Hong, K. Y. Park, H. Kim, S. W. Kim, K. Kang, *Chem. Rev.* **2014**, *114*, 11788.
[4] Y. Wang, J. Yi, Y. Xia, *Adv. Energy Mater.* **2012**, *2*, 830.
[5] Z. Yang, J. Zhang, M. C. Kintner-Meyer, X. Lu, D. Choi, J. P. Lemmon, J. Liu, *Chem. Rev.* **2011**, *111*, 3577.
[6] H. Pan, Y.-S. Hu, L. Chen, *Energy Environ. Sci.* **2013**, *6*, 2338.
[7] H. Kim, H. Kim, Z. Ding, M. H. Lee, K. Lim, G. Yoon, K. Kang, *Adv. Energy Mater.* **2016**, *6*, 1600943.
[8] M. M. Thackeray, C. Wolverton, E. D. Isaacs, *Energy Environ. Sci.* **2012**, *5*, 7854.
[9] B. Dunn, H. Kamath, J.-M. Tarascon, *Science* **2011**, *334*, 18.
[10] V. Etacheri, R. Marom, R. Elazari, G. Salitra, D. Aurbach, *Energy Environ. Sci.* **2011**, *4*, 3243.
[11] W. Li, J. R. Dahn, D. S. Wainwright, *Science* **1994**, *264*, 1115.
[12] S.-W. Kim, D.-H. Seo, X. Ma, G. Ceder, K. Kang, *Adv. Energy Mater.* **2012**, *2*, 710.
[13] M. D. Slater, D. Kim, E. Lee, C. S. Johnson, *Adv. Funct. Mater.* **2013**, *23*, 947.
[14] N. Yabuuchi, K. Kubota, M. Dahbi, S. Komaba, *Chem. Rev.* **2014**, *114*, 11636.
[15] P. G. Dicken, A. M. Chippindale, S. J. Hibble, *Solid State Ionics* **1989**, *34*, 79.
[16] M. Toupin, T. Brousse, D. Belanger, *Chem. Mater.* **2004**, *16*, 3184.
[17] H. Xia, Y. Shirley Meng, G. Yuan, C. Cui, L. Lu, *Electrochem. Solid-State Lett.* **2012**, *15*, A60.
[18] L. Athouel, F. Moser, R. Dugas, O. Crosnier, D. Belanger, T. Brousse, *J. Phys. Chem. C.* **2008**, *112*, 7270.
[19] J. F. Whitacre, T. Wiley, S. Shanbhag, Y. Wenzhuo, A. Mohamed, S. E. Chun, E. Weber, D. Blackwood, E. Lynch-Bell, J. Gulakowski, C. Smith, D. Humphreys, *J. Power Sources* **2012**, *213*, 255.
[20] X. Shan, D. S. Charles, Y. Lei, R. Qiao, G. Wang, W. Yang, M. Feygenson, D. Su, X. Teng, *Nat. Commun.* **2016**, *7*, 13370.
[21] J. F. Whitacre, A. Tevar, S. Sharma, *Electrochem. Commun.* **2010**, *12*, 463.
[22] D. J. Kim, R. Ponraj, A. G. Kannan, H.-W. Lee, R. Fathi, R. Ruffo, C. M. Mari, D. K. Kim, *J. Power Sources* **2013**, *244*, 758.
[23] A. D. Tevar, J. F. Whitacre, *J. Electrochem. Soc.* **2010**, *157*, A870.
[24] Y. Wang, L. Mu, J. Liu, Z. Yang, X. Yu, L. Gu, Y.-S. Hu, H. Li, X.-Q. Yang, L. Chen, X. Huang, *Adv. Energy Mater.* **2015**, *5*, 1501005.
[25] Y. H. Jung, S. T. Hong, D. K. Kim, *J. Electrochem. Soc.* **2013**, *160*, A897.
[26] Q. T. Qu, Y. Shi, S. Tian, Y. H. Chen, Y. P. Wu, R. Holze, *J. Power Sources* **2009**, *194*, 1222.
[27] N. Karikalan, C. Karuppiah, S. M. Chen, M. Velmurugan, P. Gnanaprakasam, *Chem. - Eur. J.* **2017**, *23*, 2379.
[28] Z. Hou, X. Li, J. Liang, Y. Zhu, Y. Qian, *J. Mater. Chem. A.* **2015**, *3*, 1400.
[29] B. H. Zhang, Y. Liu, Z. Chang, Y. Q. Yang, Z. B. Wen, Y. P. Wu, R. Holze, *J. Power Sources* **2014**, *253*, 98.
[30] Y. Liu, Y. Qiao, W. Zhang, H. Xu, Z. Li, Y. Shen, L. Yuan, X. Hu, X. Dai, Y. Huang, *Nano Energy* **2014**, *5*, 97.
[31] Y. Liu, Y. Qiao, X. Lou, X. Zhang, W. Zhang, Y. Huang, *ACS Appl. Mater. Interfaces* **2016**, *8*, 14564.
[32] Z. Chen, J. R. Dahn, *J. Electrochem. Soc.* **2002**, *149*, A1184.
[33] C. Masquelier, L. Croguennec, *Chem. Rev.* **2013**, *113*, 6552.
[34] F. Sanz, C. Parada, J. M. Rojo, C. Ruız-Valero, *Chem. Mater.* **2001**, *13*, 1334.
[35] S. M. Wood, C. Eames, E. Kendrick, M. S. Islam, *J. Phys. Chem. C.* **2015**, *119*, 15935.
[36] M. Nose, H. Nakayama, K. Nobuhara, H. Yamaguchi, S. Nakanishi, H. Iba, *J. Power Sources* **2013**, *234*, 175.
[37] J. Y. Jang, H. Kim, Y. Lee, K. T. Lee, K. Kang, N.-S. Choi, *Electrochem. Commun.* **2014**, *44*, 74.
[38] M. Nose, S. Shiotani, H. Nakayama, K. Nobuhara, S. Nakanishi, H. Iba, *Electrochem. Commun.* **2013**, *34*, 266.
[39] G. Ali, J. H. Lee, D. Susanto, S. W. Choi, B. W. Cho, K. W. Nam, K. Y. Chung, *ACS Appl. Mater. Interfaces* **2016**, *8*, 15422.
[40] A. J. Fernández-Ropero, D. Saurel, B. Acebedo, T. Rojo, M. Casas-Cabanas, *J. Power Sources* **2015**, *291*, 40.
[41] W. Song, X. Ji, Y. Zhu, H. Zhu, F. Li, J. Chen, F. Lu, Y. Yao, C. E. Banks, *ChemElectroChem* **2014**, *1*, 871.
[42] Q. Zhang, C. Liao, T. Zhai, H. Li, *Electrochim. Acta.* **2016**, *196*, 470.
[43] J. Dong, G. Zhang, X. Wang, S. Zhang, C. Deng, *J. Mater. Chem. A.* **2017**, *5*, 18725.
[44] H. Gao, J. B. Goodenough, *Angew. Chem.* **2016**, *55*, 12768.
[45] H. Wang, T. Zhang, C. Chen, M. Ling, Z. Lin, S. Zhang, F. Pan, C. Liang, *Nano Res.* **2017**, *1*, 1.
[46] P. R. Kumar, Y. H. Jung, J. E. Wang, D. K. Kim, *J. Power Sources* **2016**, *324*, 421.
[47] H. Qin, Z. P. Song, H. Zhan, Y. H. Zhou, *J. Power Sources* **2014**, *249*, 367.
[48] Y. H. Jung, C. H. Lim, J.-H. Kim, D. K. Kim, *RSC Adv.* **2014**, *4*, 9799.
[49] K. Iraya, I. Uchida, *Acc. Chem. Res.* **1986**, *19*, 162.
[50] A. B. Bocarsly, S. J. Sinha, *Electroanal. Chem.* **1982**, *137*, 157.
[51] S. K. Mohn, E. W. Grabner, *Electrochim. Acta* **1989**, *34*, 1265.
[52] C. D. Wessells, S. V. Peddada, R. A. Huggins, Y. Cui, *Nano Lett.* **2011**, *11*, 5421.
[53] C. D. Wessells, S. V. Peddada, M. T. McDowell, R. A. Huggins, Y. Cui, *J. Electrochem. Soc.* **2012**, *159*, A98.
[54] C. D. Wessells, M. T. McDowell, S. V. Peddada, M. Pasta, R. A. Huggins, Y. Cui, *ACS Nano* **2012**, *6*, 1688.
[55] P. Jiang, H. Shao, L. Chen, J. Feng, Z. Liu, *J. Mater. Chem. A* **2017**, *5*, 16740.
[56] D. J. Kim, Y. H. Jung, K. K. Bharathi, S. H. Je, D. K. Kim, A. Coskun, J. W. Choi, *Adv. Energy Mater.* **2014**, *4*, 1400133.
[57] D. Cai, X. Yang, B. Qu, T. Wang, *Chem. Commun.* **2017**, *53*, 6780.
[58] J.-H. Lee, G. Ali, D. H. Kim, K. Y. Chung, *Adv. Energy Mater.* **2017**, *7*, 1601491.
[59] X. Wu, Y. Cao, X. Ai, J. Qian, H. Yang, *Electrochem. Commun.* **2013**, *31*, 145.
[60] X. Y. Wu, M. Y. Sun, Y. F. Shen, J. F. Qian, Y. L. Cao, X. P. Ai, H. X. Yang, *ChemSusChem* **2014**, *7*, 407.
[61] X. Wu, M. Sun, S. Guo, J. Qian, Y. Liu, Y. Cao, X. Ai, H. Yang, *ChemNanoMat* **2015**, *1*, 188.
[62] X. Wu, Y. Luo, M. Sun, J. Qian, Y. Cao, X. Ai, H. Yang, *Nano Energy* **2015**, *13*, 117.
[63] A. J. Fernández-Ropero, M. J. Piernas-Muñoz, E. Castillo-Martínez, T. Rojo, M. Casas-Cabanas, *Electrochim. Acta* **2016**, *210*, 352.
[64] B. Paulitsch, J. Yun, A. S. Bandarenka, *ACS Appl. Mater. Interfaces* **2017**, *9*, 8107.
[65] L.-P. Wang, P.-F. Wang, T.-S. Wang, Y.-X. Yin, Y.-G. Guo, C.-R. Wang, *J. Power Sources* **2017**, *355*, 18.
[66] M. Minakshi, D. Meyrick, D. Appadoo, *Energy Fuels* **2013**, *27*, 3516.
[67] F. Yu, S. Zhang, C. Fang, Y. Liu, S. He, J. Xia, J. Yang, N. Zhang, *Ceram. Int.* **2017**, *43*, 9960.

[68] X. Dong, L. Chen, J. Liu, S. Haller, Y. Wang, Y. Xia, *Sci. Adv.* **2016**, *2*, e1501038.
[69] S. I. Park, I. Gocheva, S. Okada, J.-i. Yamaki, *J. Electrochem. Soc.* **2011**, *158*, A1067.
[70] J. Y. Luo, W. J. Cui, P. He, Y. Y. Xia, *Nat. Chem.* **2010**, *2*, 760.
[71] W. Wu, J. Yan, A. Wise, A. Rutt, J. F. Whitacre, *J. Electrochem. Soc.* **2014**, *161*, A561.
[72] G. Pang, C. Yuan, P. Nie, B. Ding, J. Zhu, X. Zhang, *Nanoscale* **2014**, *6*, 6328.
[73] X. Li, X. Zhu, J. Liang, Z. Hou, Y. Wang, N. Lin, Y. Zhu, Y. Qian, *J. Electrochem. Soc.* **2014**, *161*, A1181.
[74] A. I. Mohamed, N. J. Sansone, B. Kuei, N. R. Washburn, J. F. Whitacre, *J. Electrochem. Soc.* **2015**, *162*, A2201.
[75] B. Zhao, Q. Wang, S. Zhang, C. Deng, *J. Mater. Chem. A.* **2015**, *3*, 12089.
[76] F. Sagane, *J. Electrochem. Soc.* **2016**, *163*, A2835.
[77] B. Zhao, B. Lin, S. Zhang, C. Deng, *Nanoscale* **2015**, *7*, 18552.
[78] T.-F. Hung, W.-H. Lan, Y.-W. Yeh, W.-S. Chang, C.-C. Yang, J.-C. Lin, *ACS Sustainable Chem. Eng.* **2016**, *4*, 7074.
[79] Z. Guo, Y. Zhao, Y. Ding, X. Dong, L. Chen, J. Cao, C. Wang, Y. Xia, H. Peng, Y. Wang, *Chem* **2017**, *3*, 348.
[80] W. Wu, S. Shabhag, J. Chang, A. Rutt, J. F. Whitacre, *J. Electrochem. Soc.* **2015**, *162*, A803.
[81] A. I. Mohamed, J. F. Whitacre, *Electrochim. Acta* **2017**, *235*, 730.
[82] L. W. Shacklette, T. E. Toth, N. S. Murthy, R. H. Baughman, *J. Electrochem. Soc.* **1985**, *132*, 1529.
[83] C. Herold, D. Billaud, *Solid State Ionics* **1990**, *40*, 985.
[84] Q. Zhao, Y. Lu, J. Chen, *Adv. Energy Mater.* **2017**, *7*, 1601792.
[85] W. Deng, Y. Shen, J. Qian, H. Yang, *Chem. Commun.* **2015**, *51*, 5097.
[86] T. Gu, M. Zhou, M. Liu, K. Wang, S. Cheng, K. Jiang, *RSC Adv.* **2016**, *6*, 53319.
[87] G. Milczarek, O. Inganas, *Science* **2012**, *335*, 1468.
[88] Y. Wu, R. Zeng, J. Nan, D. Shu, Y. Qiu, S.-L. Chou, *Adv. Energy Mater.* **2017**, *7*, 1700278.
[89] Y. Liang, Y. Jing, S. Gheytani, K. Y. Lee, P. Liu, A. Facchetti, Y. Yao, *Nat. Mater.* **2017**, *16*, 841.
[90] Q. T. Qu, L. L. Liu, Y. P. Wu, R. Holze, *Electrochim. Acta* **2013**, *96*, 8.
[91] C. Deng, S. Zhang, Z. Dong, Y. Shang, *Nano Energy* **2014**, *4*, 49.
[92] L. Ke, J. Dong, B. Lin, T. Yu, H. Wang, S. Zhang, C. Deng, *Nanoscale* **2017**, *9*, 4183.
[93] M. Pasta, C. D. Wessells, N. Liu, J. Nelson, M. T. Mcdowell, R. A. Huggins, M. F. Toney, Y. Cui, *Nat. Commun.* **2014**, *5*, 3007.
[94] Y. Liu, B. H. Zhang, S. Y. Xiao, L. L. Liu, Z. B. Wen, Y. P. Wu, *Electrochim. Acta* **2014**, *116*, 512.
[95] F. Zhang, W. Li, X. Xiang, M. Sun, *Chem. - Eur. J.* **2017**, *23*, 12944.
[96] Y. Wang, J. Liu, B. Lee, R. Qiao, Z. Yang, S. Xu, X. Yu, L. Gu, Y. S. Hu, W. Yang, K. Kang, H. Li, X. Q. Yang, L. Chen, X. Huang, *Nat. Commmun.* **2015**, *6*, 6401.
[97] Z. Li, D. Young, K. Xia, W. C. Carter, Y. M. Chiang, *Adv. Energy Mater.* **2013**, *3*, 290.
[98] K. Xu, *Chem. Rev.* **2004**, *104*, 4303.
[99] L. Smith, B. Dunn, *Science* **2015**, *350*, 918.
[100] A. von Wald Cresce, M. Gobet, O. Borodin, J. Peng, S. M. Russell, E. Wikner, A. Fu, L. Hu, H.-S. Lee, Z. Zhang, *J. Phys. Chem. C.* **2015**, *119*, 27255.
[101] Z. Li, D. B. Ravnsbæk, K. Xiang, Y.-M. Chiang, *Electrochem. Commun.* **2014**, *44*, 12.
[102] L. Chen, J. Liu, Z. Guo, Y. Wang, C. Wang, Y. Xia, *J. Electrochem. Soc.* **2016**, *163*, A904.
[103] M. Vujković, M. Mitrić, S. Mentus, *J. Power Sources* **2015**, *288*, 176.
[104] B. Zhang, Y. Liu, X. Wu, Y. Yang, Z. Chang, Z. Wen, Y. Wu, *Chem. Commun.* **2014**, *50*, 1209.
[105] L. Suo, O. Borodin, T. Gao, M. Olguin, J. Ho, X. Fan, C. Luo, C. Wang, K. Xu, *Science* **2015**, *350*, 938.
[106] Y. Yamada, K. Usui, K. Sodeyama, S. Ko, Y. Tateyama, A. Yamada, *Nat. Energy* **2016**, *1*, 16129.
[107] K. Nakamoto, R. Sakamoto, M. Ito, A. Kitajou, S. Okada, *Electrochemistry* **2017**, *85*, 179.
[108] K. Nakamoto, Y. Kano, A. Kitajou, S. Okada, *J. Power Sources* **2016**, *327*, 327.
[109] R.-S. Kühnel, D. Reber, C. Battaglia, *ACS Energy Lett.* **2017**, *2*, 2005.
[110] X. Xiang, W. Li, F. Zhang, X. Zhang, *ChemElectroChem* **2017**, *4*, 1.
[111] H. Tomiyasu, H. Shikata, K. Takao, N. Asanuma, S. Taruta, Y. Y. Park, *Sci. Rep.* **2017**, *7*, 45048.
[112] P. R. Kumar, Y. H. Jung, B. Moorthy, D. K. Kim, *J. Electrochem. Soc.* **2016**, *163*, A1484.
[113] M. Pasta, R. Y. Wang, R. Ruffo, R. Qiao, H.-W. Lee, B. Shyam, M. Guo, Y. Wang, L. A. Wray, W. Yang, *J. Mater. Chem. A* **2016**, *4*, 4211.
[114] L. Suo, O. Borodin, Y. Wang, X. Rong, W. Sun, X. Fan, S. Xu, M. A. Schroeder, A. V. Cresce, F. Wang, C. Yang, Y.-S. Hu, K. Xu, C. Wang, *Adv. Energy Mater.* **2017**, *7*, 1701189.
[115] F. Wang, Y. Lin, L. Suo, X. Fan, T. Gao, C. Yang, F. Han, Y. Qi, K. Xu, C. Wang, *Energy Environ. Sci.* **2016**, *9*, 3666.
[116] Z. Hou, X. Zhang, X. Li, Y. Zhu, J. Liang, Y. Qian, *J. Mater. Chem. A* **2017**, *5*, 730.
[117] H. Che, S. Chen, Y. Xie, H. Wang, K. Amine, X.-Z. Liao, Z.-F. Ma, *Energy Environ. Sci.* **2017**, *10*, 1075.
[118] J. Wojciechowski, L. Kolanowski, A. Bund, G. Lota, *J. Power Sources* **2017**, *368*, 18.
[119] M. Wang, M. Tang, S. Chen, H. Ci, K. Wang, L. Shi, L. Lin, H. Ren, J. Shan, P. Gao, Z. Liu, H. Peng, *Adv. Mater.* **2017**, *29*, 1703882.
[120] H. Maleki, G. Deng, I. K. Haller, A. Anani, J. N. Howard, *J. Electrochem. Soc.* **2000**, *147*, 4470.
[121] Y. Shi, X. Zhou, G. Yu, *Acc. Chem. Res.* **2017**, *50*, 2642.
[122] Y. Shi, M. Wang, C. Ma, Y. Wang, X. Li, *Nano Lett.* **2015**, *15*, 6276.